

Reaction mechanism for atmospheric pressure plasma treatment of cysteine in solution

Jordyn Polito¹ , María J Herrera Quesada² , Katharina Stapelmann² 
and Mark J Kushner^{3,*} 

¹ Department of Chemical Engineering, University of Michigan, Ann Arbor, MI 48109, United States of America

² Department of Nuclear Engineering, North Carolina State University, Raleigh, NC 27695, United States of America

³ Department of Electrical Engineering and Computer Science, University of Michigan, Ann Arbor, MI 48109, United States of America

E-mail: mjkush@umich.edu

Received 19 April 2023, revised 14 June 2023

Accepted for publication 26 June 2023

Published 6 July 2023



CrossMark

Abstract

Mechanisms for the cold atmospheric plasma (CAP) treatment of cells in solution are needed for more optimum design of plasma devices for wound healing, cancer treatment, and bacterial inactivation. However, the complexity of organic molecules on cell membranes makes understanding mechanisms that result in modifications (i.e. oxidation) of such compounds difficult. As a surrogate to these systems, a reaction mechanism for the oxidation of cysteine in CAP activated water was developed and implemented in a 0-dimensional (plug-flow) global plasma chemistry model with the capability of addressing plasma-liquid interactions. Reaction rate coefficients for organic reactions in water were estimated based on available data in the literature or by analogy to gas-phase reactions. The mechanism was validated by comparison to experimental mass-spectrometry data for COST-jets sustained in He/O₂, He/H₂O and He/N₂/O₂ mixtures treating cysteine in water. Results from the model were used to determine the consequences of changing COST-jet operating parameters, such as distance from the substrate and inlet gas composition, on cysteine oxidation product formation. Results indicate that operating parameters can be adjusted to select for desired cysteine oxidation products, including nitrosylated products.

Keywords: atmospheric pressure plasma, plasma treatment of organics, reaction mechanism in solution, mass spectroscopy, modeling

(Some figures may appear in colour only in the online journal)

* Author to whom any correspondence should be addressed.



Original content from this work may be used under the terms of the [Creative Commons Attribution 4.0 licence](https://creativecommons.org/licenses/by/4.0/). Any further distribution of this work must maintain attribution to the author(s) and the title of the work, journal citation and DOI.

1. Introduction

Cold atmospheric pressure plasmas (CAPs) have potential applications in plasma medicine including cancer treatment [1, 2], chronic wound healing [3], disinfection [4, 5], and medical device decontamination [6]. A variety of well-characterized CAP devices have been used for plasma medical applications, including dielectric barrier discharges, atmospheric pressure plasma jets, and plasma needles [7–10]. These devices are either ‘touching’, in which the plasma is in direct contact with the target, or ‘non-touching’ in which reactive species generated in the plasma transport across a non-powered region to reach the target. Plasma jet devices for biomedical applications are generally sustained in either argon or helium with additives or impurities (i.e. air, oxygen, water) that result in generation of reactive oxygen and nitrogen species (RONS) in the plasma.

The RONS produced in these plasma jets include some of the same RONS involved in biological processes in living organisms where they play an active role in redox biology [11]. RONS, generated by CAP or a living system, are known to affect proteins [12] particularly proteins with the thiol (–SH)-containing amino acid cysteine which is prone to oxidation and nitrosylation [13, 14]. The low molecular weight protein glutathione (GSH), for example, is the major cellular cysteine-containing protein participating in cellular redox reactions [15]. Crucial biological processes involve the thiol redox state. The inflammatory extracellular signaling protein high mobility group box 1 (HMGB1), for example, contains three redox-sensitive cysteine residues [16]. Depending on the dynamic redox state of each of the cysteine residues, the protein fulfills different functions. The consequences of plasma treatment of proteins *in vivo* could be, to a certain extent, transported or preserved via thiol group oxidation [17]. Oxidative modifications of biomolecules have the potential to modulate and control downstream physiological processes [18].

Cystine (RSSR), a commonly found product after plasma treatment, contains a disulfide bridge, a key structural element essential for protein structure and function [19]. Cystine is a sensitive sensor of the redox state of a cell [19] which can be further oxidized or nitrosylated. These molecules can lead to bioactive derivatives that have anti-proliferative effects on cancer cells [20], playing a role in the nitric oxide pathway with implications for wound healing, cancer biology, and cardiac functioning [21–23]. A range of products, including non-stable transient products, can be found after plasma treatment [14, 21]. Bioactive reactive sulfur species (e.g. cyst(e)ine sulfoxides and cysteine-S-sulfonate) have the potential to influence cellular redox balance [20, 24].

Given the large number of in-solution RONS produced by CAP, and the many reactions that may occur with living cells, isolating specific reaction pathways is challenging [25, 26]. The amino acid cysteine has been used in studies of CAP interacting with water-based solutions as a surrogate for biological models, due to its amino, carboxyl, and thiol groups that are common in biological macromolecules, and cell membranes

in particular [21, 27–29], and the biological relevance of the molecule, as discussed above. Developing mechanisms for in-solution interactions of RONS with simpler amino acids provides a baseline for understanding such interactions with living cells.

Developing an in-solution reaction mechanism for CAP produced RONS interactions with cysteine will benefit from a combined experimental and computational approach. Cysteine interactions with RONS have been modeled by Lackmann *et al* [30] using molecular dynamics (MD) simulations. The MD simulations included interactions of reactants that may be produced by two plasma jet sources, the kINPen sustained in argon [31] and the European Cooperation for Science and Technology (COST)-jet sustained in helium/argon mixtures [32]. Cysteine oxidation was initiated by OH_{aq} or NO_{aq} at the thiol (–SH) site on the cysteine molecule. (The subscript ‘aq’ denotes an in-solution species, to differentiate from their gas phase analogues). Interactions with $\text{H}_2\text{O}_{2\text{aq}}$, $\text{O}_{2\text{aq}}$, and $\text{O}_{3\text{aq}}$ were also addressed, but were found to be less important than interactions with OH_{aq} and NO_{aq} on the short timescales that could be addressed with MD (≤ 10 ps). A detailed mechanism was produced, which included branching ratios of cysteine oxidation products formed after interactions of cysteine or cysteine intermediate products with RONS. However, due to the computational limitations of MD, longer timescale interactions on the order of seconds or minutes could not be resolved.

Computational models with the ability to address timescales consistent with experimental treatment times (seconds to minutes) would aid in further understanding of plasma-assisted modifications of organic molecules in solutions. Recent measurements have shown that atomic O_{aq} is one of the most abundant ROS produced by CAP sources sustained in mixtures containing oxygen impurities, and so its interactions with organic molecules should also be considered [33, 34].

In this paper, we discuss results from computational and experimental investigations in which we propose a reaction mechanism for the COST-jet treatment of cysteine in water solutions. A 0-dimensional (0D) global plasma chemistry model was used in a plug-flow mode to simulate the gas-phase reactive species densities and fluxes that come into contact with ambient air in the gap between the reactor outlet and continue to the liquid surface. The gas-phase fluxes impinge on a 1 mm thick solution of cysteine in water. A liquid reaction mechanism that accounts for transport across the gas-liquid interface and liquid-phase reactions was coupled to the gas phase plasma-chemistry model, providing densities of in-liquid species after plasma treatment. The reaction mechanism was validated with experimental mass spectroscopy (MS) measurements from the He/O_2 and $\text{He}/\text{H}_2\text{O}$ COST-jet treatment of cysteine in a water solution. Experiments were also performed for solutions treated by the COST-jet sustained in $\text{He}/\text{N}_2/\text{O}_2$ to produce nitrosylated cysteine products, in addition to oxidation products. The results from the model were used to investigate reaction pathways and mechanisms responsible for the production of cysteine oxidation products as a function of plasma operating parameters

including distance between the reactor outlet and the liquid surface, oxygen inlet flow rate, and nitrogen inlet flow rate. Results indicate that some degree of control over the formation of specific products can be achieved by leveraging these plasma parameters.

The experimental methods used to investigate He/N₂/O₂ COST-jet treatment of cysteine in solution are described in section 2. A description of the model and the cysteine reaction mechanism are in sections 3 and 4. A comparison of the model results against experimental data for validation of the reaction mechanism is contained in section 5. Plasma and liquid properties produced by the model for base-case conditions are in section 6. Results, including comparison of the model with experimental mass spectroscopy measurements are discussed in section 7. Conclusions are in section 8.

2. Description of the experiments

2.1. Plasma source

The experiments utilize the atmospheric pressure COST reference microplasma jet (the COST-jet), which has been previously described in detail by Golda *et al* [32]. The COST-jet is a capacitively coupled plasma that operates at a frequency of 13.56 MHz. The source has two 30 mm long electrodes positioned 1 mm apart, resulting in an active plasma region measuring 1 mm × 1 mm × 30 mm. Helium was used as the primary inlet gas. Experiments used for validation of the model kept a total gas flow of 1 slm for the two gas mixtures of He/H₂O = 99.75/0.25 and He/O₂ = 99.4/0.6. For the He/H₂O mixture, dry helium was passed through a bubbler before being mixed with additional dry helium downstream to produce the desired mole fractions. To reduce impurities, the helium and oxygen (research grade ARC3 PurityPlus 5.0) were delivered through stainless steel tubing. The nitrogen containing gas mixture for the base case was He/N₂/O₂ = 99.0/0.8/0.2. The power deposition was kept constant at 750 ± 10 mW and was continuously monitored with integrated current and voltage probes.

2.2. Sample treatment

To investigate the consequences of plasma treatment of biologically important molecules, the amino acid cysteine was used as a surrogate. The L-form of cysteine was sourced from Alfa Aesar (L-Cysteine A10435, ≥98%) and dissolved in high performance liquid chromatography (HPLC) grade water to a final concentration of 100 μg ml⁻¹. One milliliter of these solutions was then transferred to 12-well plates producing a solution depth of 1 mm and exposed to the COST-jet effluent at a gap distance of 4 mm. For each gas mixture, control samples were also taken where the cysteine solution was only exposed to the respective gas flow without igniting the plasma for a duration equal to the maximum treatment time used. All experiments were performed in triplicate.

2.3. Mass spectroscopy

The chemical changes that occurred in cysteine due to plasma treatment were experimentally analyzed using mass spectroscopy (MS). An autosampler vial was filled with 100 μl of each 1 ml sample. A UPLC-MS/MS method was used, utilizing a Thermo Vanquish LC instrument (Thermo Fisher Scientific) coupled to a Thermo Orbitrap Exploris 480 mass spectrometer (Thermo Fisher Scientific) with a heated electrospray ionization source. Chromatographic separation was accomplished with a Waters BEH Amide column (2.1 × 100 mm, 1.8 μM) that was maintained at 45 °C. A linear gradient of mobile phase A (H₂O + 0.1% FA [formic acid]) and mobile phase B (MeCN + 0.1% FA) was used: 0–0.1 min (99% B, 0.4 ml min⁻¹), 0.1–7 min (99%–30% B, 0.4 ml min⁻¹), 7–10 min (99% B, 0.4 ml min⁻¹). Samples were analyzed as 2 μl injections in positive ion mode (spray voltage 3.5 kV, vaporizer temperature 350 °C, ion transfer tube temperature °C, sheath gas 50 a.u., sweep gas 1 a.u., and aux gas 10 a.u.) with a mass range of m/z 60–1000. Mass spectrometer 1 (MS1) data were collected with a resolving power of 60 000 and an automatic gain control target of 1 × 10⁻⁶. Mass spectrometer 2 (MS2) data were collected with a resolving power of 30 000, cycle time of 0.6 s, and stepped higher-energy collision dissociation energy of (30, 50, 150 eV). The raw data were imported into Skyline, an open-source MS analysis software package [35], for peak integration and selection using targeted data processing.

3. Description of the model

GlobalKin is a 0D plasma chemistry model that includes the capability to address plasma-liquid interactions across an interface. Detailed descriptions of *GlobalKin* and methods used to address plasma-liquid interactions can be found in [36, 37] and so are discussed only briefly here. In short, species densities in the gas phase are determined according to continuity equations that account for sources and losses due to electron impact and heavy particle reactions, diffusion to the walls, and gas flow. The electron energy equation is solved to provide a reactor averaged or position dependent electron temperature. Electron energy distributions are determined by solving the stationary Boltzmann equation over a range of E/N values. Rate coefficients obtained from these distribution functions are stored in a look-up table as functions of electron temperature. The look-up tables are interpolated throughout the execution of the model to provide electron impact reaction rate and transport coefficients at the current electron temperature. The table is periodically updated to reflect changes in gas composition.

Gas flow is approximated using a plug-flow approach. The plug-flow approximation is valid for subsonic flow systems having constant pressure with there being little diffusion in the flow direction. In the plug-flow approach, gas flows down the length of the reactor as a slug of gas having cross-sectional area $A = WD$ where W is the electrode width and D is the distance

Table 1. Gas phase species included in plasma chemistry model.

Hydrogen Species ^{a, b}
H, H [*] , H ⁺ , H ⁻ , H ₂ , H ₂ (<i>r</i>), H ₂ (<i>v</i>), H ₂ ⁺ , H ₂ [*] , H ₃ ⁺
Oxygen Species ^{a, b}
O ₂ , O ₂ (<i>r</i>), O ₂ (<i>v</i>), O ₂ [*] , O ₂ (¹ S), O ₂ ⁺ , O ₂ ⁻ , O, O [*] , O ⁺ , O ⁻ , O ₃ , O ₃ [*] , O ₃ ⁻ , O ₄ ⁺
Nitrogen Species ^{a, b}
N ₂ , N ₂ (<i>r</i>), N ₂ (<i>v</i>), N ₂ [*] , N ₂ ⁺ , N ₃ ⁺ , N ₄ ⁺ , N, N [*] , N ⁺
Helium Species ^a
He, He ⁺ , He, He(2 ¹ S), He(2 ³ S), He(2 ³ P), He(2 ¹ P), He(3P), He(3S), He ₂ [*]
Heterogeneous Species ^{a, b}
OH, OH [*] , OH ⁻ , H ₂ O, H ₂ O(<i>v</i>), H ₂ O ⁺ , HO ₂ , H ₂ O ₂ , H ₃ O ⁺ , NO, NO ⁺ , NO ₂ , NO ₂ ⁺ , NO ₂ ⁻ , NO ₃ , NO ₃ ⁻ , N ₂ O, N ₂ O(<i>v</i>), N ₂ O ₃ , N ₂ O ₄ , N ₂ O ₅ , NH, HNO, HNO ₂ , HNO ₃ , HNO ₄ , H ₄ O ₂ ⁺ , H ₂ O ₃ ⁺ , H ₃ O ₂ ⁺ , H ₂ NO ₂ ⁺ , H ₄ NO ₃ ⁺ , H ₆ NO ₄ ⁺ , H ₂ NO ⁺ , HeH ⁺

^a * denotes an excited state atom or molecule.

^b (*r*) and (*v*) denote rotationally and vibrationally excited molecules, respectively.

between the electrodes. Transport perpendicular to the flow direction to the walls of the reactor is addressed by ambipolar diffusion for charged particles and fundamental mode free diffusion for neutral particles. Integration in time is converted to integration in space along the flow direction by translating $d/dx = (\frac{1}{v})d/dt$ for flow speed v . As such, there is not a spatial mesh. Values are recorded after the spatial location changes by fixed increments, here about every 70 μm . The speed of the plug is a function of the inlet flow rate (sccm), gas-density, and the reactor cross-sectional area. The flow speed is adjusted with changes in total gas number density due to gas heating or reactions to maintain a constant pressure.

When using plug-flow, input power (W cm^{-3}) is specified as a function of reactor position in the flow direction. In this investigation, the specified power density is constant along the length of the reactor with the exception of a 1 mm ramp-up distance at the beginning of the reactor and 2 mm ramp-down distance at the end of the reactor. The power density profile is normalized such that the integral over the entire reactor volume of power density equals the total desired input power. Although the COST-jet operates with a radio frequency power supply, the power along the axis is not time varying—the power is the average over the RF period.

GlobalKin includes a liquid module that accounts for the interaction of the gas-phase plasma in contact with a liquid layer. All gas-phase species have solvated liquid counterparts. A separate liquid-phase reaction mechanism is included for these solvated species. The gas-phase species and liquid-phase species interact only at the gas-liquid interface. Transport is limited to diffusion into or out of the liquid layer. Electrons and heavy charged species solvate into the liquid with unity probability where most positive ions charge exchange with water produce to $\text{H}_2\text{O}^+_{\text{aq}}$ which then rapidly converts to $\text{H}_3\text{O}^+_{\text{aq}}$. Penning ionization or dissociative excitation transfer occurs with excited states of He incident onto the liquid. That said, the plume of the COST-jet onto the liquid is nearly charge free (by design) and excited states of He are largely quenched prior to reaching the liquid. As a result, the dynamics of charge particles (or Penning processes) due to their fluxes from the

gas phase onto the liquid are not particularly important in this investigation.

Neutral gas-phase species diffuse into and out of the liquid with a probability determined by the Henry's law equilibrium constant h_i for that species. The probability that a neutral gas-phase species will solvate into the liquid can be thought of as a sticking coefficient at the liquid interface, $S_{i,l}$,

$$S_{i,l} = \frac{h_i n_{i,g} - n_{i,l}}{h_i n_{i,g}}. \quad (1)$$

where $n_{i,l}$ is the density of species i in the liquid and $n_{i,g}$ is the density of species i in the gas. If the gas-phase and liquid phase are in equilibrium, then $n_{i,l} = n_{i,g} \times h_i$. Species will solvate from the gas phase into the liquid as long as $\frac{n_{i,l}}{n_{i,g}} < h_i$. When $\frac{n_{i,l}}{n_{i,g}} > h_i$ the liquid is super-saturated and net transport is from the liquid into the gas-phase. The Henry's law constants used in this work are shown in table 1. Liquid species densities are determined by a species continuity equation that is similar to that used for the gas-phase. Sources and losses due to liquid phase reactions, solvation, and evaporation are accounted for in the liquid species density calculation.

Several observations of plasma-jet induced vortexes in liquid have been reported, for example Stancampiano *et al* [38]. Such vortexing is not resolved in the global model. Creating these vortexes typically requires a deep solution, whereas the solution used in the experiment is only 1 mm thick. An important component of the forces creating vortexes is electrohydrodynamic forces which are not important for the COST-jet as the plume is largely neutral. As a result, we do not expect there to be significant vortexing for our conditions. If vortexing did occur, then there would be more mixing in the solution which would actually better align with the global model.

4. Reaction mechanism

The gas-phase mechanism for a He/O₂/N₂ atmospheric pressure plasma has been discussed in detail in previous works

Table 2. Henry's law constants.

Species	Dimensionless Henry's law constant	Comments
H, H*	6.48×10^{-3}	a, b
H ₂ , H ₂ (<i>r</i>), H ₂ (<i>v</i>), H ₂ *	1.80×10^{-2}	a
OH, OH(A ² Σ)	6.20×10^2	a
HO ₂	1.32×10^5	
H ₂ O ₂	1.92×10^6	
O ₂ , O ₂ (<i>v</i>), O ₂ (<i>r</i>), O ₂ (¹ S)	3.24×10^{-2}	a
O, O*	2.00×10^1	c
O ₃ , O ₃ *	3.00×10^{-1}	a
N ₂ , N ₂ (<i>r</i>), N ₂ (<i>v</i>), N ₂ [*] , N, N*	1.60×10^{-2}	a, b
He, He(2 ¹ S), He(2 ³ S), He(2 ³ P), He(2 ¹ P), He(3P), He(3S), He ₂ *	9.42×10^{-3}	a, b
NO	4.40×10^{-2}	
NO ₂	2.80×10^{-1}	
NO ₃	4.15×10^1	
N ₂ O, N ₂ O(<i>v</i>)	5.99×10^{-1}	a
N ₂ O ₃	6.00×10^2	
N ₂ O ₄	3.69×10^1	
N ₂ O ₅	4.85×10^1	
NH	1.47×10^3	d
HNO ₂ , HNO	1.15×10^3	a
HNO ₃	4.80×10^6	
HNO ₄	3.47×10^6	

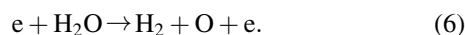
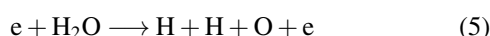
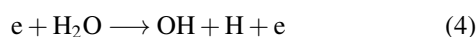
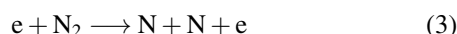
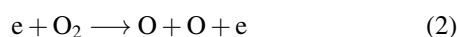
^a Value corresponds to the first species in the list. Other species listed were assumed to have the same Henry's law constant.

^b Excited states rapidly quench to ground state in water. Henry's law saturation is not expected.

^c Adjusted from [29] for consistency with experimental measurements of atomic O density in liquid for similar COST-jet systems [48, 49].

^d Approximated as NH₃.

[37, 39, 40]. Briefly, electron impact dissociation of O₂, N₂, and H₂O (when a water impurity is included in the inlet) are responsible for generating some RONS (e.g. O, OH) and the reactive products needed to form other RONS,



Electron energy is primarily lost through inelastic collisions that produce electronically, rotationally, or vibrationally excited states of O₂, N₂, and H₂O (O₂(*r*), O₂(*v*), O₂^{*}, O₂(¹S), N₂(*r*), N₂(*v*), N₂^{*}, H₂O(*v*)). Electronically excited states of N₂ (N₂^{*}) are dissociatively quenched by O₂ to produce O atoms, and participate in reactions with O to form NO. O₃ is formed as a result of three-body reactions of O and O₂. The 79 gas-phase species included in this work are listed in table 2. As is common in modeling of complex plasma chemistry, excitation to several excited states is lumped into producing a single state, here denoted with *, which is usually the lowest lying state with the longest lifetime. This practice acknowledges that higher excited states will relax or be quenched on times shorter than those of interest. Typically, only the lowest lying, meta-stable states survive in the plume to reach the liquid.

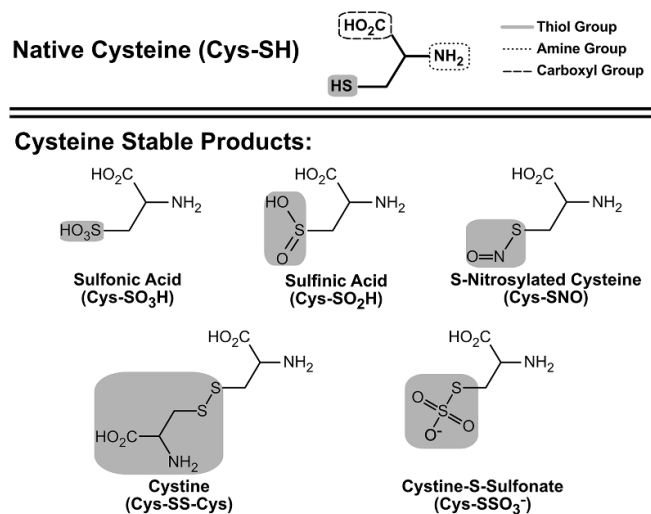


Figure 1. Molecular structure of native cysteine and its stable oxidation products.

Every gas-phase species has a liquid-phase counterpart. The liquid-phase mechanism has been discussed previously in [36, 41]. Neutral species from the gas-phase solvate into the liquid-phase as described in the previous section. Reactive neutrals can combine in the liquid to form more stable molecules (e.g. OH_{aq}, H₂O_{2aq}, O_{3aq}, HNO_{3aq}, NO_{3aq}). Solvated RONS and RONS produced by plasma-assisted liquid reactions react with organic molecules in the liquid to produce oxidated and nitrosylated organic products.

Table 3. Cysteine-liquid reaction mechanism.

Cysteine species			
Cys-SH	Cysteine		
Cys-S	Thiol radical		
Cys=S	Cys(-2 H), intermediate product. Reconfiguration of S after H abstraction.		
Cys-SOH	Sulfenic acid		
Cys-SO ₂ H	Sulfinic acid		
Cys-SO ₃ H	Sulfonic acid		
Cys-S(OH) ₂	Intermediate product. 2 OH additions to S after H abstraction.		
Cys-SOH ₂	Intermediate product. Direct OH addition to SH group.		
Cys-S=O	Intermediate product. O double bonded to S after H abstraction.		
Cys-S-S-Cys	Cystine		
Cys-SONO	Double bonded O, N double bonded O addition to S after H abstraction		
Cys-SNO	N double bonded O addition to S after H abstraction		
Cys-S-S	Product of radical attack on cystine		
Cys(-2 H)	Product of radical attack on cystine		
Cys-S-S-O ₂	Intermediate product in the formation of Cysteine-S-Sulfonate		
Cys-S-S-O ₃ ⁻	Cysteine-S-Sulfonate		
SH	Abstracted thiol group		

	Reaction	Reaction rate coefficient ^a	Comments
<i>Initiation reactions</i>			
1	$\text{OH}_{(\text{aq})} + \text{Cys-SH} \rightarrow \text{H}_2\text{O}_{(\text{aq})} + \text{Cys-S}^\bullet$	1.68×10^{-17}	b
2	$\text{HO}_{2(\text{aq})} + \text{Cys-SH} \rightarrow \text{H}_2\text{O}_{2(\text{aq})} + \text{Cys-S}^\bullet$	5.65×10^{-16}	b
3	$\text{OH}_{(\text{aq})} + \text{Cys-SH} \rightarrow \text{H}_2\text{O}_{(\text{aq})} + \text{SH} + \text{Cys}(-2 \text{ H})$	1.00×10^{-18}	est.
4	$\text{O}_{(\text{aq})} + \text{Cys-SH} \rightarrow \text{OH}_{(\text{aq})} + \text{SH} + \text{Cys}(-2 \text{ H})$	2.00×10^{-18}	est.
5	$\text{O}_{(\text{aq})} + \text{Cys-SH} \rightarrow \text{OH}_{(\text{aq})} + \text{Cys-S}$	1.68×10^{-15}	b
6	$\text{O}^-_{(\text{aq})} + \text{Cys-SH} \rightarrow \text{OH}^-_{(\text{aq})} + \text{Cys-S}$	1.68×10^{-20}	est.
<i>Intermediate product formation</i>			
7	$\text{O}_{(\text{aq})} + \text{Cys-S}^\bullet \rightarrow \text{O}_{(\text{aq})} + \text{Cys} = \text{S}$	5.60×10^{-13}	est.
8	$\text{O}^-_{(\text{aq})} + \text{Cys-S}^\bullet \rightarrow \text{O}^-_{(\text{aq})} + \text{Cys} = \text{S}$	5.60×10^{-20}	est.
9	$\text{OH}_{(\text{aq})} + \text{Cys-S} \rightarrow \text{OH}_{(\text{aq})} + \text{Cys} = \text{S}$	5.60×10^{-14}	b
10	$\text{OH}^-_{(\text{aq})} + \text{Cys-S} \rightarrow \text{OH}^-_{(\text{aq})} + \text{Cys} = \text{S}$	5.60×10^{-20}	est.
11	$\text{O}_{2(\text{aq})} + \text{Cys-S} \rightarrow \text{O}_{2(\text{aq})} + \text{Cys} = \text{S}$	4.68×10^{-15}	b
12	$\text{O}_2^-_{(\text{aq})} + \text{Cys-S} \rightarrow \text{O}_2^-_{(\text{aq})} + \text{Cys} = \text{S}$	1.00×10^{-20}	b
13	$\text{O}_{3(\text{aq})} + \text{Cys-S} \rightarrow \text{O}_{2(\text{aq})} + \text{Cys-S} = \text{O}$	8.31×10^{-16}	b
14	$\text{OH}_{(\text{aq})} + \text{Cys-S} \rightarrow \text{Cys-SOH}_2$	2.80×10^{-17}	b
15	$\text{O}_{3(\text{aq})} + \text{Cys-SOH}_2 \rightarrow \text{H}_2\text{O}_{(\text{aq})} + \text{O}_{2(\text{aq})} + \text{Cys-S} = \text{O}$	2.08×10^{-16}	b
16	$\text{OH}_{(\text{aq})} + \text{Cys-SOH} \rightarrow \text{Cys-S(OH)}_2$	5.60×10^{-17}	b
17	$\text{OH}_{(\text{aq})} + \text{Cys-S-S-Cys} \rightarrow \text{OH}_{(\text{aq})} + \text{Cys-S} + \text{Cys-S-S}$	2.00×10^{-15}	est.
18	$\text{SO}_{2(\text{aq})} + \text{Cys-S} \rightarrow \text{Cys-S-S-O}_2$	3.49×10^{-13}	b
19	$\text{NO}_{(\text{aq})} + \text{Cys-S} = \text{O} \rightarrow \text{Cys-SONO}$	5.00×10^{-19}	est.
<i>Sulfenic acid formation</i>			
20	$\text{H}_2\text{O}_{2(\text{aq})} + \text{Cys-SH} \rightarrow \text{H}_2\text{O}_{(\text{aq})} + \text{Cys-SOH}$	4.68×10^{-22}	est.
21	$\text{OH}_{(\text{aq})} + \text{Cys-S} \rightarrow \text{OH}_{(\text{aq})} + \text{Cys-SOH}$	5.60×10^{-13}	b
22	$\text{O}_{3(\text{aq})} + \text{Cys-SOH}_2 \rightarrow \text{O}_{2(\text{aq})} + \text{OH}_{(\text{aq})} + \text{Cys-SOH}$	6.23×10^{-16}	b
<i>Sulfinic acid formation</i>			
23	$\text{O}_{(\text{aq})} + \text{Cys-S(OH)}_2 \rightarrow \text{OH}_{(\text{aq})} + \text{Cys-SO}_2\text{H}$	1.12×10^{-15}	est.
24	$\text{O}^-_{(\text{aq})} + \text{Cys-S(OH)}_2 \rightarrow \text{OH}^-_{(\text{aq})} + \text{Cys-SO}_2\text{H}$	1.12×10^{-18}	est.
25	$\text{OH}_{(\text{aq})} + \text{Cys-S} = \text{O} \rightarrow \text{OH}_{(\text{aq})} + \text{Cys-SO}_2\text{H}$	1.00×10^{-17}	b
26	$\text{OH}_{(\text{aq})} + \text{Cys-S(OH)}_2 \rightarrow \text{H}_2\text{O}_{(\text{aq})} + \text{Cys-SO}_2\text{H}$	1.12×10^{-17}	est.
27	$\text{O}_{2(\text{aq})} + \text{Cys-S(OH)}_2 \rightarrow \text{HO}_{2(\text{aq})} + \text{Cys-SO}_2\text{H}$	4.68×10^{-17}	est.

(Continued.)

Table 3. (Continued.)

<i>Sulfonic acid formation</i>			
28	$O_{(aq)} + \text{Cys-SO}_2\text{H} \rightarrow H_{(aq)} + \text{Cys-SO}_3\text{H}$	5.60×10^{-14}	est.
29	$OH_{(aq)} + \text{Cys-SO}_2\text{H} \rightarrow H_{(aq)} + \text{Cys-SO}_3\text{H}$	5.60×10^{-15}	b
30	$O_{2(aq)} + \text{Cys-SO}_2\text{H} \rightarrow O_{(aq)} + \text{Cys-SO}_3\text{H}$	4.68×10^{-17}	b
31	$H_2O_{2(aq)} + \text{Cys-SO}_2\text{H} \rightarrow H_2O_{(aq)} + \text{Cys-SO}_3\text{H}$	4.68×10^{-20}	b
<i>Cystine formation</i>			
32	$\text{Cys-S} + \text{Cys-S} \rightarrow \text{Cys-S-S-Cys}$	1.00×10^{-10}	b
<i>Cystine-S-sulfonate formation</i>			
33	$HSO_3^-(aq) + \text{Cys-S-S-Cys} \rightarrow \text{Cys-SH} + \text{Cys-S-S-O}_3^-$	1.00×10^{-18}	est.
34	$HSO_3^-(aq) + \text{Cys-SH} \rightarrow H_{2(aq)} + \text{Cys-S-S-O}_3^-$	1.00×10^{-15}	est.
35	$OH_{(aq)} + \text{Cys-S-SO}_2 \rightarrow H^+_{(aq)} + \text{Cys-S-S-O}_3^-$	1.00×10^{-15}	est.
<i>Cysteine-SNO formation</i>			
36	$NO_{(aq)} + \text{Cys-S} \rightarrow \text{Cys-SNO}$	5.60×10^{-19}	est.
<i>Additional reactions</i>			
37	$O_{2(aq)} + \text{SH} \rightarrow SO_2^-(aq) + H^+_{(aq)}$	1.24×10^{-11}	b
38	$H_2O_{2(aq)} + \text{SH} \rightarrow HO_{2(aq)} + H_2S_{(aq)}$	5.00×10^{-15}	b
39	$\text{Cys}(-2\text{H}) + \text{SH} + H_{(aq)} \rightarrow \text{Cys}$	1.00×10^{-35}	est.
40	$\text{Cys}(-2\text{H}) + H_2\text{S} \rightarrow \text{Cys}$	1.00×10^{-15}	est.

^a Reaction rate coefficients have units of $\text{cm}^3 \text{s}^{-1}$.

^b Reaction rate is approximated from an analogous gas-phase reaction with a long chain alkane from the NIST database [44] or from analogous reactions in solution from the NIST solutions [45] database and adjusted to match experimental measurements.

Cysteine is an organic compound containing a carboxyl group ($-\text{COOH}$), an amine group ($-\text{NH}_2$), and a thiol group ($-\text{SH}$). (See figure 1.) The cysteine reaction mechanism includes 17 cysteine-derived species and 40 liquid-phase reactions of RONS with cysteine. The reaction mechanism and reaction rate coefficients used in this work are shown in table 3. Only reactions with the thiol group of the cysteine molecule are considered in this work. The sulfur atom in the thiol group is highly reactive in comparison to the other parts of the cysteine molecule, leading to preferential interaction of RONS with the thiol site [21, 29]. The presence of the carboxyl group leads to resonance stabilization of the cysteine molecule which contributes to a reduction in reactivity at sites other than the thiol site [42].

Similar to the gas-phase oxidation of long-chain alkanes [43], the liquid-phase oxidation of the cysteine thiol site can be considered a three-step mechanism. Oxidation begins with abstraction of the H atom from the thiol site by O_{aq} , O_{aq}^- , OH_{aq} , OH_{aq}^- , or HO_{2aq} to form a thiol radical site. Reactions of RONS at the thiol radical site result in short-lived intermediate products that can undergo rearrangement or subsequent reactions with RONS to form stable oxidation products. In this work an oxidation product is considered stable when its lifetime is long enough to enable experimental detection [30]. We consider cysteine sulfenic acid ($\text{Cys-SO}_2\text{H}$), cysteine sulfonic acid ($\text{Cys-SO}_3\text{H}$), cysteine-S-sulfonate (Cys-SSO_3^-), cystine (Cys-S-S-Cys), and nitrosylated cysteine (Cys-SNO) to be stable compounds. The structures of these molecules are shown in figure 1. (Since Cys- species only exist in solution, the 'aq' suffix will not be used in the following text).

The reaction mechanism of RONS with cysteine shown in table 3 was initially based on MD simulations by Lackmann *et al* [30]. Reaction rate coefficients for oxidations of organic molecules in solution are largely unavailable and so have been estimated based on analogous gas-phase reactions of RONS with alkanes taken from the National Institute of Science and Technology (NIST) Chemical Kinetics Database [44]. In the few cases where they are available, reaction rate coefficients of RONS with the native cysteine molecule were taken from the NIST Solutions database [45]. Reaction rate coefficients have been adjusted to account for differences in the interactions of molecules in the liquid-phase rather than the gas-phase and to achieve consistency with experiments. In general, gas-phase reaction rate coefficients produced shorter times for cysteine depletion and oxidation in the liquid-phase than observed experimentally. These smaller rate coefficients in large part reflect transport limits in the liquid compared to the gas phase.

5. Validation of the reaction mechanism

Stapelmann *et al* [46] tracked several COST-jet produced ROS from the gas-phase to the liquid phase to predict their impact on the modification of cysteine molecules in a water solution. MS was used to show trends in depletion of the native cysteine and formation of cysteine-derived oxidation products in heavy water ($H_2^{18}O$) over five minutes of plasma treatment for two gas mixtures, $\text{He}/O_2 = 99.4/0.6$ and $\text{He}/H_2O = 99.75/0.25$. The gas mixtures were chosen to control the dominant

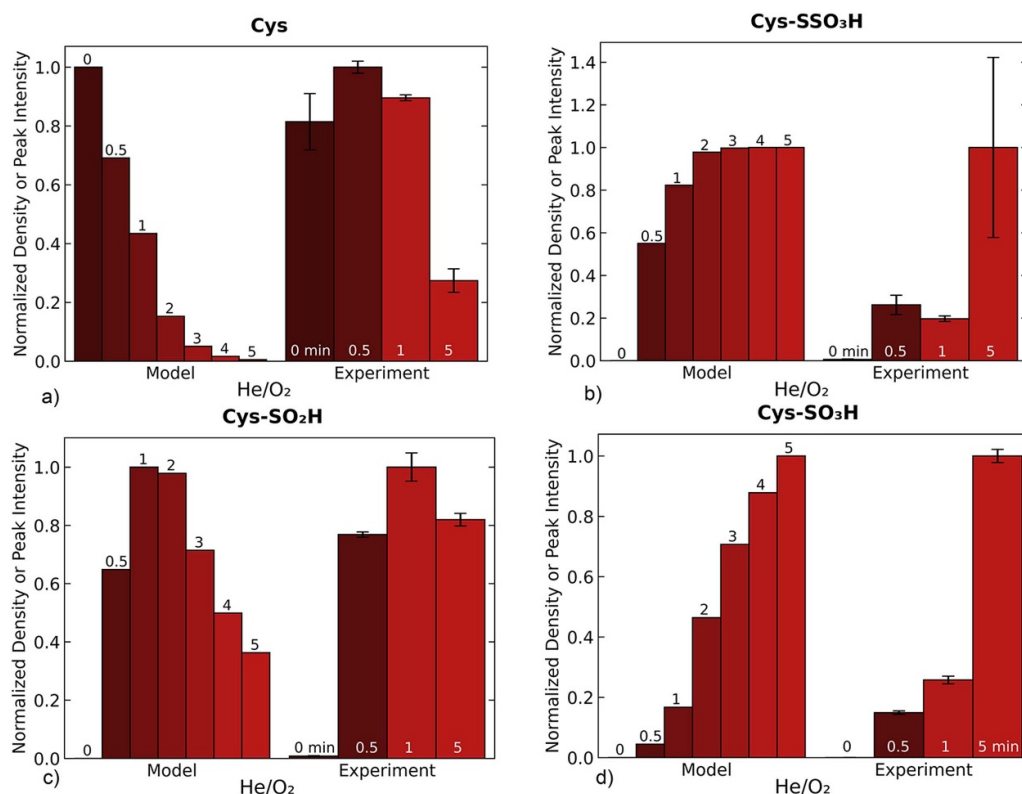


Figure 2. Comparison of trends in (a) native cysteine depletion and (b)–(d) cysteine oxidation product formation between model and experiments for the COST-jet treatment using a He/O₂ = 99.4/0.6 gas mixture as a function of plasma exposure time. Values (model-predicted number density or mass spectrometry-produced peak intensity) have been normalized to 1.

plasma-produced ROS (O in He/O₂; OH and H₂O₂ in He/H₂O) fluxes to the liquid. The stable cysteine oxidation products considered were cysteine-S-sulfonate (Cys-SSO₃H), cysteine sulfenic acid (Cys-SO₂H), and cysteine sulfonic acid (Cys-SO₃H). The combination product cystine (Cys-S-S-Cys) was also measured. The authors found significant differences in the reaction pathways between treating the solution with the COST-jet sustained in He/O₂ and He/H₂O. Treatment with the COST-jet using the He/O₂ mixture resulted in preferential formation of irreversible oxidation products (i.e. Cys-SO₃H) while treatment by the COST-jet using the He/H₂O mixture favored reversible oxidation products (i.e. Cys-SO₂H). The authors attributed the difference in product formation to the origin of the ROS responsible for the modification. ROS known in redox biology, like OH in the He/H₂O mixture, caused more reversible oxidation products while ROS unknown to nature, i.e. O in the He/O₂ mixture, caused irreversible reaction products.

5.1. He/O₂ and He/H₂O COST-jet treatment

Results from the Stapelmann *et al* study [46] have been reproduced in this section to provide validation for the reaction mechanism discussed in section 4. The MS-produced peak intensity measurements for cysteine-derived oxidation products formed over a five-minute treatment period by exposure to the effluent from COST-jets sustained in He/O₂ and He/H₂O which are shown alongside model-produced

densities in figures 2 and 3. Values have been normalized to one to provide a more direct comparison of the trends in product formation over time between the experiments and the model. The model uses the same reaction mechanism as discussed in section 4. Only the gas composition has been adjusted to match the gas composition used in the experiments.

Overall, trends predicted by the model are in good agreement with the measured values. For treatment of cysteine using the COST-jet sustained in He/O₂ (figure 2), cysteine is significantly depleted after five minutes of plasma treatment as H is abstracted from the thiol group by ROS (O_{aq}, OH_{aq}, HO_{2,aq}) to form thiol radical sites. Thiol radical sites are converted to intermediate oxidation products by subsequent reactions with ROS. Intermediate products can then be converted to stable oxidation products by reactions with RONS or with reactions involving O_{2,aq}. The reaction mechanism relating the formation pathways of the cysteine oxidation products to the fluxes of plasma-produced RONS is discussed in section 7.

Cys-S-SO₃H and Cys-SO₃H (irreversible oxidation products) are preferentially produced after 2–3 min of plasma treatment, which is consistent with the results by Bhoj and Kushner [39]. The model also accurately predicts the trend in generation of Cys-SO₂H, which forms over the first minute of plasma treatment, then is depleted over the next four minutes as Cys-SO₂H is converted to Cys-SO₃H by reactions with solvated ROS.

When exposed to the COST-jet sustained in He/H₂O, Cys-SO₃H and Cys-S-SO₃H are also formed, though neither are

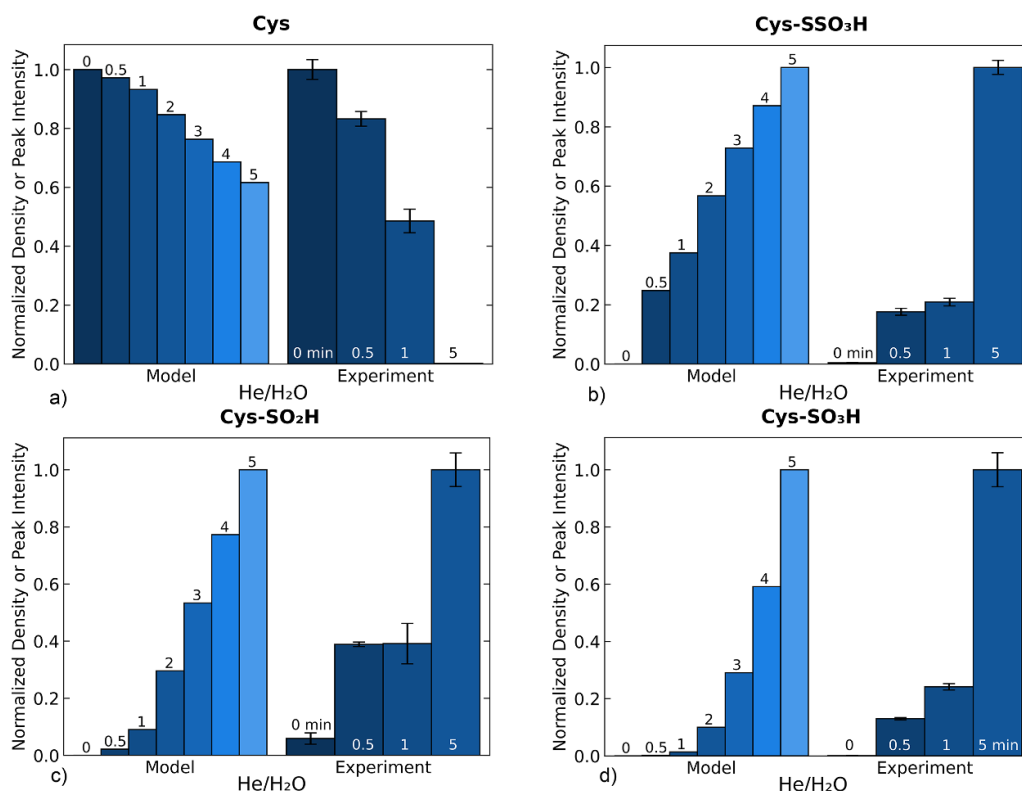


Figure 3. Comparison of trends in (a) native cysteine depletion and (b)–(d) cysteine oxidation product formation between model and experiments for the COST-jet sustained in a He/H₂O = 99.75/0.25 gas mixture as a function of plasma exposure time. Values (model-predicted number density or mass spectrometry-produced peak intensity) have been normalized to 1.

formed preferentially. Unlike treatment by the COST-jet sustained in He/O₂, where Cys-SO₂H is eventually depleted, Cys-SO₂H forms continuously when using the He/H₂O mixture. This result indicates that a higher fluence of plasma-produced ROS, O in particular, is needed to promote conversion to Cys-SO₃H. The fluences of RONS required to produce cysteine oxidation products are discussed in section 7. Though not shown in figure 3, cystine (Cys-S-S-Cys) is preferentially formed by treatment with the COST-jet sustained in He/H₂O. Hydrogen is abstracted from the thiol (–SH) site of the cysteine molecule to create a thiol radical site. In the absence of significant densities of ROS, and especially at early treatment times, two thiol sites will react to form Cys-S-S-Cys.

6. Base case plasma and liquid species properties

The reactor configuration used for the results in this section is based on the experimental setup discussed in section 2. The COST-jet sustained in He/O₂ has been extensively characterized [32]. Typical O atom densities for 0.2–1.0% O₂ admixtures have been reported to be between 1 and 3 × 10¹⁵ cm^{−3} while O₃ densities increase from 1 × 10¹⁴ cm^{−3} to 1 × 10¹⁵ cm^{−3} as the percent of O₂ increases [47–49]. The COST-jet is most often operated in a power range between a few hundred milliwatts and a few watts, which yields electron densities on the order of a few times 10¹⁰ cm^{−3} [50].

The model considers the radio-frequency (RF) powered, 1 atm COST-jet operated in He/N₂/O₂ mixtures with a constant power of 750 mW. The base case is 1010 sccm of a feed gas consisting of He/N₂/O₂ = 99/0.8/0.2 with a 1 ppm water impurity. The gas flows through the top of the reactor and moves vertically down the length of the reactor (3 cm) and across the gap between the reactor and liquid (4 mm). The gap between the powered and grounded electrode is 1 mm and the width of the electrodes is 1 mm, yielding a plasma with a cross-sectional area of 1 mm². The plasma is assumed to be uniform over the electrode cross-sectional area. There is a 4 mm gap between the reactor outlet and the liquid surface in which the reactor effluent comes into contact with ambient air. In this plug flow approach, the entrainment of ambient air into the effluent is approximated by adding humid air (N₂/O₂/H₂O = 79/20/1) with a flow rate of 10 sccm into the mixture as the gas exits the discharge channel.

The treated liquid is a 1 mm thick solution of water containing 100 μg ml^{−1} cysteine (5 × 10¹⁷ cm^{−3} cysteine molecules). The liquid initially has a pH = 7 and is initially saturated with atmospheric gases.

6.1. Plasma properties

The densities of gas phase species predicted by the model for the base case conditions are shown in figure 4. The average electron density in the plasma channel predicted by the model is 3 × 10¹⁰ cm^{−3} and the average electron temperature

is 2.2 eV. (Here, electron temperature is 2/3 of the average electron energy, obtained from the electron energy distribution that in most cases is non-Maxwellian.) These values are consistent with experimentally measured values for the COST-jet sustained in He/O₂ [50]. RONS including O, O₃, NO, OH, and HO₂ are produced in the powered region and exit the reactor at 3.0 cm to mix with ambient air in the gap above the liquid. Atomic oxygen is formed predominantly through electron impact dissociation of molecular oxygen or through dissociative excitation transfer to O₂ or excited state O₂ from excited state N₂. The predicted atomic oxygen density ($4 \times 10^{15} \text{ cm}^{-3}$) is consistent with experimentally reported values of atomic oxygen measured in the He/O₂ COST-jet [48, 49]. O₃ ($2 \times 10^{14} \text{ cm}^{-3}$) is formed primarily through three-body reactions of O and O₂. The predominant nitrogen-containing RONS is NO ($4 \times 10^{14} \text{ cm}^{-3}$). NO is formed primarily through electron impact excitation of molecular nitrogen (N₂^{*}), followed by reaction with O to produce N^{*} and NO. OH ($8 \times 10^{11} \text{ cm}^{-3}$), HO₂ ($2 \times 10^{11} \text{ cm}^{-3}$), and H₂O₂ ($1 \times 10^{10} \text{ cm}^{-3}$) are produced in the plasma region as a result of the small water impurity in the feed gas.

The densities of OH and HO₂ increase at the reactor outlet as the plasma effluent comes into contact with humid air, then decrease in the air gap due to interactions with each other to form H₂O and O₂. O₃ also increases in the air gap as O is consumed in three-body reactions with O₂ whose density increases in the effluent due to mixing with the ambient air. The maximum reactivity that can be produced in the liquid due to gas phase RONS is ultimately a function of the fluence of the RONS incident onto the liquid surface over the time of exposure. Fluence (molecules cm⁻²) is the time integral of the flux (molecules cm⁻² s⁻¹). The maximum density of RONS in the liquid is dependent upon the flux (cm⁻² s⁻¹) of gas phase RONS delivered to the liquid surface integrated over time, or the fluence (cm⁻²), of gas-phase RONS. The fluences of gas phase RONS onto the water that correspond to the densities shown in figure 4 for our conditions after five minutes of plasma treatment are: $1.4 \times 10^{13} \text{ cm}^{-2}$ H₂O₂, $5.0 \times 10^{13} \text{ cm}^{-2}$ HO₂, $2.6 \times 10^{14} \text{ cm}^{-2}$ OH, $9.1 \times 10^{14} \text{ cm}^{-2}$ O₃, $3.6 \times 10^{17} \text{ cm}^{-2}$ NO, and $4.8 \times 10^{18} \text{ cm}^{-2}$ O.

6.2. Liquid RONS production

Densities of aqueous species produced during five minutes of treatment by the COST-jet sustained in He/O₂/N₂ are shown in figure 5. Plasma produced RONS solvate into the liquid according to their Henry's Law equilibrium constants (i.e. species having higher Henry's law constants will solvate more readily than those with lower Henry's law constants). Solvation is primarily responsible for the production of reactive aqueous neutrals such as OH_{aq}, NO_{aq}, and O_{aq}. Solvation and subsequent saturation of OH_{aq}, NO_{aq}, and O_{aq} occur quickly (about 2 ms) after liquid exposure to the plasma effluent while other species such as H₂O_{2aq}, O_{3aq}, and HO_{2aq} require longer exposure (0.5 s–1 min) to saturate. Species, that as a result of aqueous reactions, become supersaturated will desolvate into the gas phase. In addition to solvation, H₂O_{2aq}

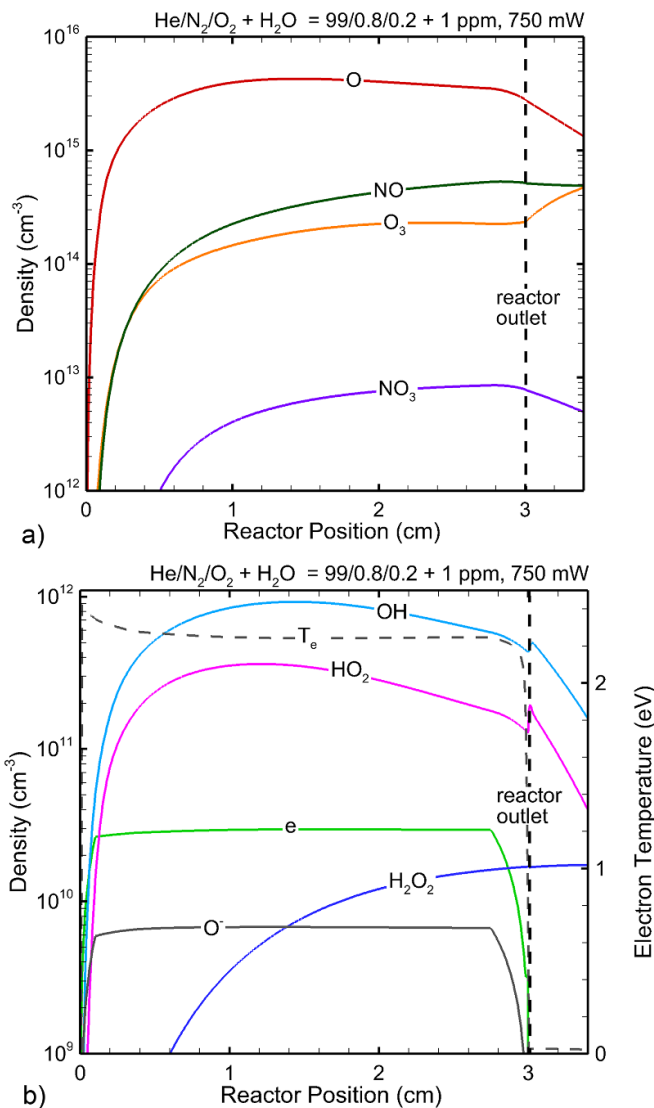
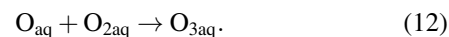
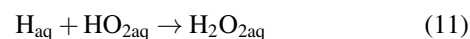
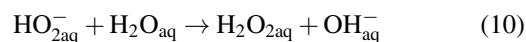
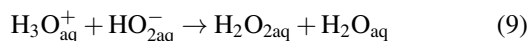
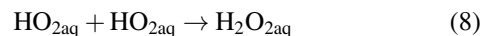
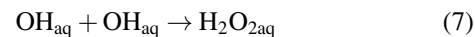


Figure 4. Base case plasma properties for COST-jet operating in 1010 sccm He/N₂/O₂ = 99/0.8/0.2 with 750 mW power deposition. (a) ROS and RNS. (b) Electron temperature and density, and ROS.

and O_{3aq} are formed through aqueous reactions of solvated ROS.



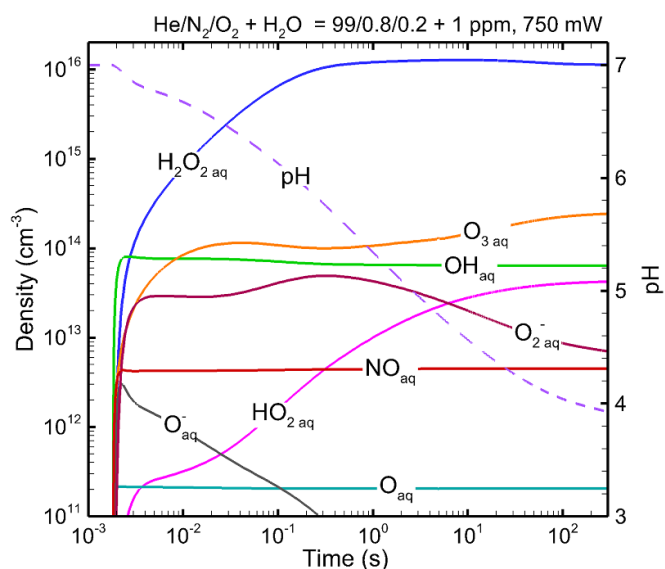
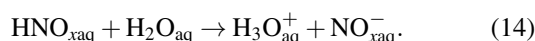


Figure 5. Base case aqueous densities for COST-jet operating in 1010 sccm He/N₂/O₂ = 99/0.8/0.2, 750 mW treating a 100 μg ml⁻¹ cysteine (5 × 10¹⁷ cm⁻³ cysteine molecules) solution.

H₂O_{2aq} and O_{3aq} are considered long-lived species as they are relatively stable (thermal decay occurs, but on timescales longer than the studied treatment time). Long-lived species can produce more reactive products over their lifetimes, either in reactions with other RONS or by slow-decay processes.

(H)NO_x species are some of the most abundant plasma-produced RONS that solvate into the liquid. The dominant gas phase RONS are NO (5 × 10¹⁴ cm⁻³) and HNO₂ (8 × 10¹² cm⁻³). NO_{aq} and NO_{2aq} reach saturation within milliseconds of treatment time. NO_{xaq} species undergo reactions with H₂O_{aq} to form HNO_{xaq}, which hydrolyzes to form H₃O⁺_{aq}.



The increase in H₃O⁺_{aq} results in a decrease of the model-predicted pH from 7 to 3.9 over the course of the five-minute treatment for the COST-jet sustained in He/O₂/N₂, whereas mixtures not containing N₂ tend to produce smaller changes in pH [51, 52]. Cysteine is stable within the pH range studied in this work and so pH does not play a direct role in the modification of the cysteine molecule [53]. However, the pH tolerances of the target molecule and surrounding system should be taken into consideration when designing plasma devices for biological treatments.

7. Formation of cysteine oxidation products

In this section, the model-predicted densities of cysteine oxidation products after plasma treatment will be discussed while varying the gap distance between the reactor exit and the liquid and the inlet gas composition. A comparison between

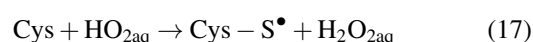
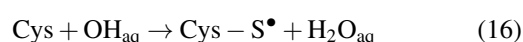
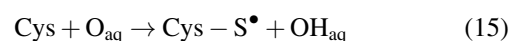
model results and experimental mass spectroscopy measurements will be presented to motivate the addition of N₂ to the gas inlet.

7.1. Base case modifications to native cysteine

Plasma jets in general, and the COST-jet in particular, potentially offer precise control over RONS delivered to a target by varying the inlet gas composition [54, 55]. For example, addition of N₂ to the COST-jet sustained in He/O₂ increases the flux of plasma-produced (H)NO_x species reaching the liquid while decreasing the inventory of O₃ formed in the plasma. However, the effects of plasma-produced (H)NO_x on the modification of biological targets in plasma treated solutions is still unclear. Experiments described in section 3 were performed to help illuminate the consequences of N₂ addition to the inlet gas on cysteine oxidation product formation. MS was performed and used for further validation of the reaction mechanism for the tri-gas conditions. Normalized model-produced densities of cysteine and several oxidation products for the base case discussed in section 6 are shown in figure 6 alongside normalized MS peak intensity measurements from experiments also performed under the base case conditions in figure 6.

The model-produced aqueous number densities of cysteine and its stable derivatives are shown in figure 7 as a function of plasma treatment time. The model predicts major cysteine depletion occurs after 10–20 s of plasma treatment. The model is initialized with the only organic molecule in the water being cysteine while the experiments naturally include cystine or other unstable products that may revert back to cysteine as a result of plasma treatment. This likely explains the differences in the severity of depletion of the native cysteine between the model and the experiments. Cystine (Cys-S-S-Cys) and Cys-SSO₃H are the first stable products to form with significant number densities (>10⁸ cm⁻³).

Short-lived O and OH solvate into the liquid and their in-water densities reach saturation within a few ms. These saturation values are not a classical Henry's law equilibrium but rather an equilibrium between the rates of solvation of these species (a source) and their reaction with the organic molecules in solution (a sink). These ROS abstract H atoms from the cysteine thiol (-SH) group to form thiol radicals. Cystine initially forms from two thiol radicals, as densities of RONS, including negative ions and long-lived species such as H₂O_{2aq}, O_{3aq}, HO_{2aq}, and NO_{xaq} increase by solvation or through aqueous reactions;



Within the first few milliseconds of plasma treatment, Cys-SSO₃H also becomes a major product.

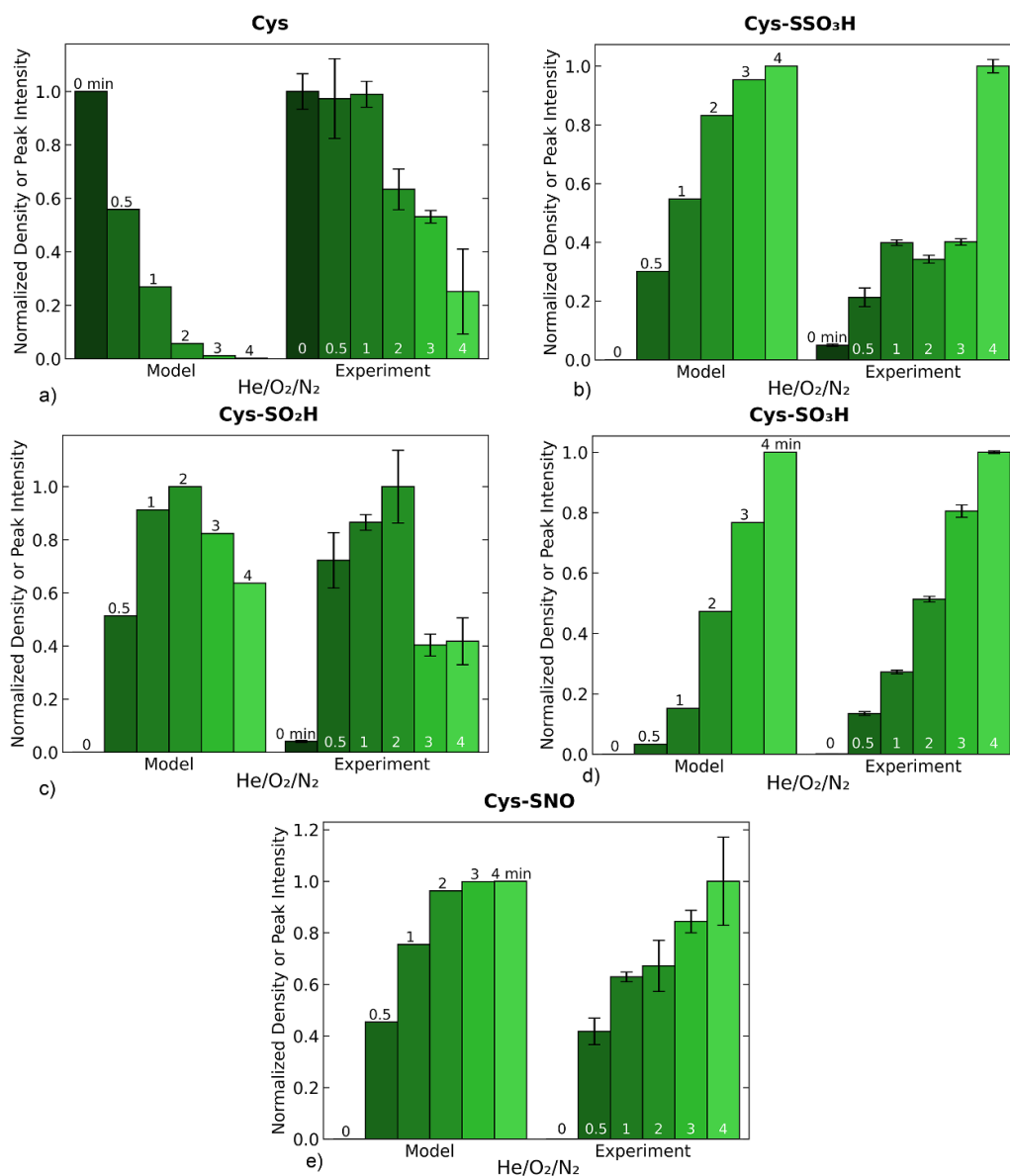
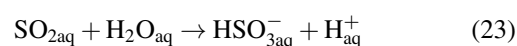
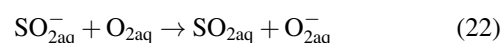
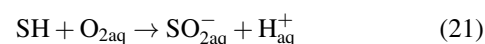
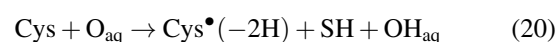
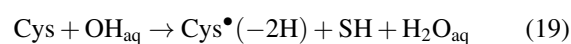


Figure 6. Comparison of trends in cysteine oxidation product formation between model and experiments for the treatment by the COST-jet sustained in $\text{He}/\text{N}_2/\text{O}_2 = 99/0.8/0.2$ gas mixture as a function of exposure time. Values (model-predicted number density or mass spectrometry-produced peak intensity) have been normalized to 1.

Several mechanisms for the formation of Cys-SSO₃H from cysteine have been proposed [56, 57]. The formation of Cys-SSO₃H may occur through cleavage of the SH group by radical attack and subsequent oxidations by SH-derived species (e.g. SO₂⁻_{aq}, SO₃⁻_{aq}) at the radical site, or through the cystine oxidation-reduction cycle. The mechanism for Cys-SSO₃H formation in this work is based on that proposed by Wende *et al* [25]. Cys-SSO₃H is represented in the mechanism as Cys-SSO₃⁻, which is conventional in oxidation-reduction chemistry. We assume that Cys-SSO₃⁻ and Cys-SSO₃H are quickly reversible in solution and use the two representations interchangeably from this point forward. The Wende mechanism suggests that in addition to abstracting H from the thiol group, O_{aq} and OH_{aq} may also remove the entire SH moiety from the cysteine molecule. SH undergoes a replacement reaction with O_{2aq} to form SO₂⁻_{aq}, which participates in charge exchange

with O_{2aq} to form SO_{2aq}. SO_{2aq} then hydrolyzes with H₂O_{aq} to form HSO₃⁻_{aq},



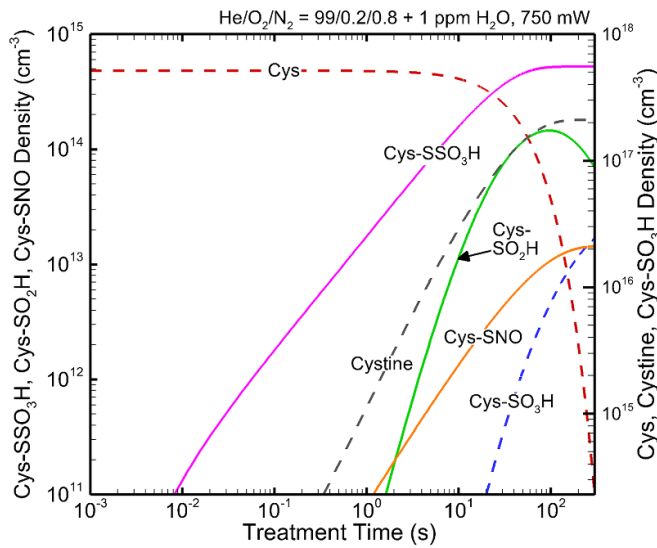
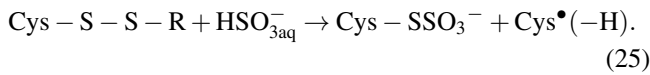
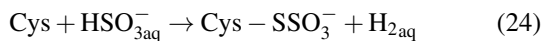


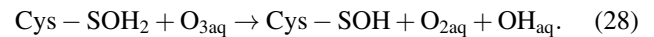
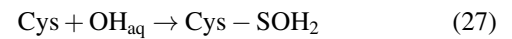
Figure 7. Model-produced number densities of cysteine oxidation products as a function of COST-jet treatment time for the base case conditions. 1010 sccm He/N₂/O₂ = 99/0.8/ 0.2, 750 mW.



After about 4 ms, HSO_{3aq}⁻ forms with high enough number density (a few times 10¹⁰ cm⁻³) to produce Cys-SSO₃H through reaction with either cysteine or Cys-S-S-Cys. Cys-SSO₃H is the primary stable oxidation product for the first 20 s of plasma treatment, after which production of sulfonic acid (Cys-SO₃H) dominates.

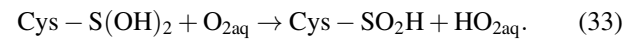
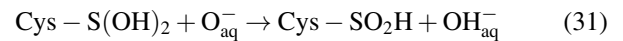
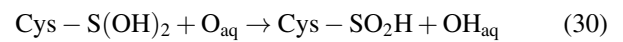
While Cys-SSO₃H and cystine are being formed, the first oxidation state of the thiol radical, sulfenic acid (Cys-SOH), is formed through a direct reaction involving OH_{aq} or a series of indirect reactions involving both OH_{aq} and O_{3aq}. The density of O_{3aq} saturates about ten times more slowly than OH, which saturates within 2 ms, as aqueous reactions contribute to the accumulation of O_{3aq}. O₃ has a saturated aqueous density of around 1 × 10¹⁴ cm⁻³ while OH has a saturated aqueous density of around 7 × 10¹³ cm⁻³. A density of 2 × 10⁸ cm⁻³ Cys-SOH forms by the time the density of OH_{aq} has reached saturation, after which the rate of formation of Cys-SOH briefly matches the rate of accumulation of O_{3aq} (from 2–20 ms).

At early treatment times (<a few ms), before saturation of most other RONS, the direct pathway to Cys-SOH formation (equation (26)) is likely dominant. Direct OH_{aq} addition to cysteine is slow compared to the formation of the Cys-SOH₂ intermediate and most other competing reactions that also consume OH_{aq}. At later times, when most other RONS are saturated, the indirect pathway for Cys-SOH formation is likely dominant,



Cys-SOH forms continuously for the first 1.5 min of treatment time before depletion starts to occur faster than formation as Cys-SOH is converted to more stable, higher oxidation products.

Conversion from Cys-SOH to sulfenic acid (Cys-SO₂H) requires the addition of OH_{aq} to Cys-SOH to form the intermediate product Cys-S(OH)₂. Subsequent reactions with O_{aq}, O_{aq}, OH_{aq}, or O_{2aq} convert the Cys-S(OH)₂ to Cys-SO₂H,



Significant quantities of Cys-SO₂H form within 20 ms of the start of plasma treatment. Cys-SO₂H accumulates over the first two minutes of plasma treatment before conversion to Cys-SO₃H overtakes Cys-SO₂H production through reaction of Cys-SO₂H with O_{aq}, OH_{aq}, O_{2aq}, or H₂O_{2aq},



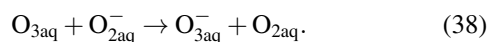
After 20 s of plasma treatment, Cys-SO₃H becomes the predominant stable oxidation product over Cys-SSO₃H. The model-predicted density of Cys-SO₃H after 5 min of plasma treatment is 2.4 × 10¹⁶ cm⁻³ and the density of Cys-SSO₃H after 5 min of plasma treatment is 5.2 × 10¹⁴ cm⁻³. Cys-SO₃H is not an easily reversible product. In living organisms, formation of Cys-SO₃H is irreversible, though formation of Cys-SO₂H and Cys-SOH can be reversed [27, 58]. This reversibility of lower oxidation states may contribute to lower densities of Cys-SOH and Cys-SO₂H in the experiments, especially at longer treatment times and under anaerobic conditions.

The oxidation of cysteine appears to be limited both by the step-wise nature of its oxidation pathways and by the hydrogen abstraction step. The hydrogen abstraction step is dependent on the solvation of fluxes of gas phase O and OH into the liquid. Cysteine oxidation product formation sensitivity to RONS production will be discussed in the following subsections.

7.2. Air gap

The distance between the reactor outlet and the liquid surface can be used as a control parameter to tune the flux of RONS reaching the liquid. The gap is adjusted in the model by extending the length over which plug flow is calculated after power is turned off at the end of the 3 cm electrode length. To emulate ambient air mixing, air is introduced to the plasma effluent at 3 cm with a flow rate that is 1% of the total inlet flowrate. Increasing the gap increases the amount of mixing between the COST-jet's effluent and the ambient air. The fluence of gas phase species onto the liquid and number densities of aqueous cysteine oxidation products after five minutes of treatment with the COST-jet sustained in the He/N₂/O₂ mixture are shown in figure 8. The densities of the aqueous species are normalized by their values for a gap of 10 mm to emphasize the trends with gap.

As the gap increases, the final number density of the cysteine increases (from $1 \times 10^{13} \text{ cm}^{-3}$ when the gap is 1 mm to $1 \times 10^{16} \text{ cm}^{-3}$ when the gap is 10 mm). This corresponds to a reduction in cysteine depletion from nearly 100% with a 1 mm gap to 49% for a gap of 10 mm. As the gap increases, air entrainment into the plasma effluent also increases. The fluence of plasma-produced short lived RONS onto the liquid decreases as reactive species are converted into more stable species in the air gap. The fluence of short-lived RONS such as O that are primarily produced in the plasma are more sensitive to changes in the gap. There are less dramatic decreases in aqueous number densities as the gap increases for RONS that can be replenished by aqueous reactions, such as O_{3aq} and OH_{aq}. Increasing the gap from 1 mm to 10 mm results in a five times reduction in saturated O_{aq} density from $3.5 \times 10^{11} \text{ cm}^{-3}$ to $7 \times 10^{10} \text{ cm}^{-3}$, whereas the reduction in OH_{aq} is only two times, from $8.6 \times 10^{13} \text{ cm}^{-3}$ to $3.6 \times 10^{13} \text{ cm}^{-3}$. The O_{3aq} density is transient, and does not reach saturation, but has maximum values at the end of treatment time ($3.6 \times 10^{14} \text{ cm}^{-3}$ for a 1 mm gap and $2 \times 10^{14} \text{ cm}^{-3}$ for a 10 mm gap). O₃ solvates into the liquid, but O_{3aq} can also be generated by aqueous reaction (equation (12)). O_{3aq} is consumed by reaction with intermediate cysteine oxidation products (reactions (13), (15), and (22) in table 3) or by charge exchange with negative ions (equation (38)) faster than it is produced by reactions with aqueous ROS for the first 6–7 s of plasma treatment time,



The rate of consumption of O_{3aq} gradually decreases over the remaining treatment time (as intermediate cysteine products are converted to higher oxidation states) while the rate of production due to aqueous reactions is nearly constant (as O_{aq} and O_{2aq} saturate). At the end of the plasma treatment time, the rate of O_{3aq} production by aqueous reaction is nearly double the rate of O_{3aq} consumption. With the gas phase density of O₃ above the water being $5 \times 10^{14} \text{ cm}^{-3}$, and a Henry's law constant of 0.3, the saturated aqueous density is $1.5 \times 10^{14} \text{ cm}^{-3}$. So the in liquid production of O_{3aq} produces slightly super-saturated conditions that result in the desolvation of O_{3aq}.

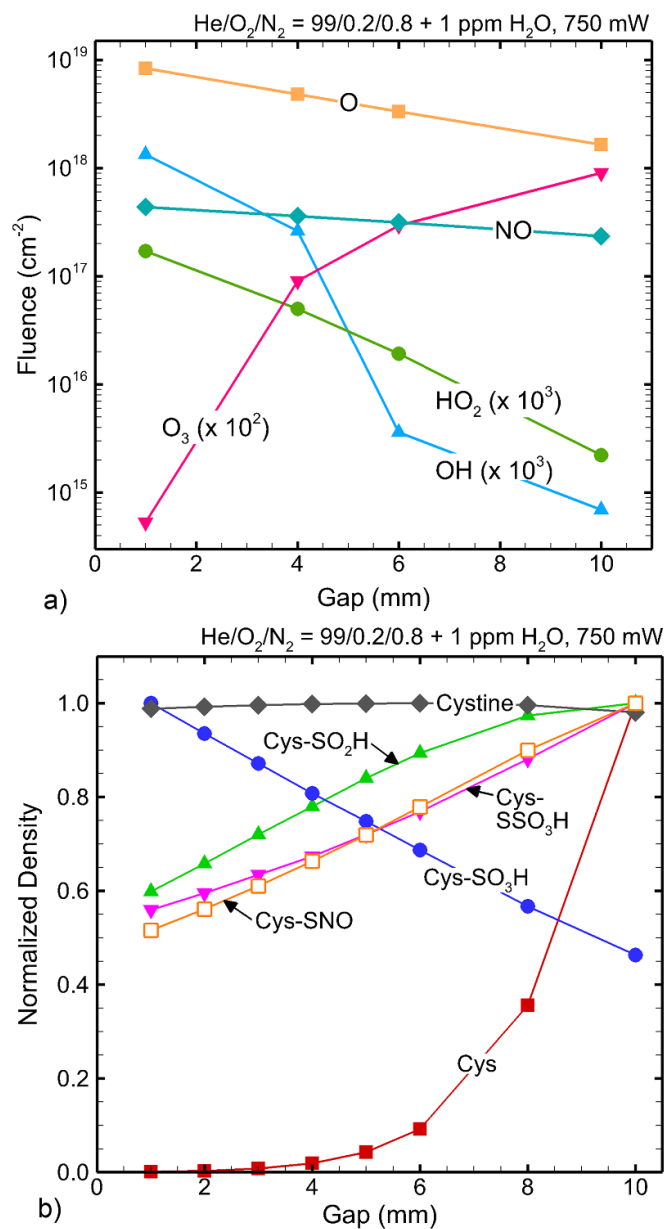


Figure 8. Reactant properties as a function of gap between nozzle and liquid. (a) Fluences of select RONS onto the liquid and (b) normalized cysteine oxidation product densities after five minutes of plasma treatment by driven the COST-jet sustained in He/N₂/O₂.

Trends in oxidation resulting from varying gap can be extended to understanding the hierarchy of RONS' importance in the production of cysteine oxidation products. As the gap increases from 1 mm to 10 mm, the final number density of Cys-SSO₃H increases from $4 \times 10^{14} \text{ cm}^{-3}$ to $8 \times 10^{14} \text{ cm}^{-3}$, Cys-SO₂H increases from $5 \times 10^{13} \text{ cm}^{-3}$ to $9 \times 10^{13} \text{ cm}^{-3}$, and Cys-SNO increases from $1 \times 10^{13} \text{ cm}^{-3}$ to $2 \times 10^{13} \text{ cm}^{-3}$. The final number density of Cys-SO₃H decreases from $3 \times 10^{16} \text{ cm}^{-3}$ to $1 \times 10^{16} \text{ cm}^{-3}$. Cys-SSO₃H formation requires O_{aq} or OH_{aq} for H abstraction, but subsequent reaction steps are driven by O_{2aq}. There is little change in the O_{2aq} density as gap distance increases due to its saturation, indicating that a reduction in short-lived aqueous ROS favors Cys-SSO₃H formation.

While not shown in figure 8, as it is not considered a stable product, the final number density of Cys-SOH also increases from $5 \times 10^{15} \text{ cm}^{-3}$ at 1 mm gap to $2 \times 10^{16} \text{ cm}^{-3}$ at 10 mm gap, though more Cys-SOH is produced in the 1 mm case than in the 10 mm case for the first 110 s of plasma treatment. The formation of Cys-SOH enables pathways to formation of higher order oxidation products. Cys-SOH formation is dependent on OH_{aq} and $\text{O}_{3\text{aq}}$ (equations (27)–(29)) while its conversion to Cys-SO₂H requires O_{aq} , $\text{O}_{\text{aq}}^{\cdot}$, OH_{aq} , or $\text{O}_{2\text{aq}}$ (equations (30)–(34)). Further conversion to Cys-SO₃H (equations (35)–(38)) requires O_{aq} , OH_{aq} , $\text{O}_{2\text{aq}}$, or $\text{H}_2\text{O}_{2\text{aq}}$. $\text{H}_2\text{O}_{2\text{aq}}$ is a long-lived aqueous species whose saturated number density decreases from $1 \times 10^{16} \text{ cm}^{-3}$ to $7 \times 10^{15} \text{ cm}^{-3}$ as the gap increases from 1 mm to 10 mm.

As the fluences of short-lived ROS onto the liquid decrease with increasing gap, the formation of Cys-SOH and Cys-SO₂H, the first and second oxidation states, are not particularly sensitive to reduction of O_{aq} . However, as Cys-SO₂H fails to be converted to Cys-SO₃H at larger gaps, formation of the third oxidation state does become sensitive to O_{aq} concentration, $\text{H}_2\text{O}_{2\text{aq}}$ concentration, or both. Based on gas phase analogues and agreement with experiment, the reaction rate coefficient of $\text{H}_2\text{O}_{2\text{aq}}$ with Cys-SO₂H (equation (37)) is 3–6 orders of magnitude smaller than reactions of Cys-SO₂H with other ROS (O_{aq} , OH_{aq}). As a result, Cys-SO₃H formation is likely most sensitive to the O_{aq} density. However, as Cys-SO₃H is the most abundant oxidation product under all conditions, fluences of O on the order of a few times 10^{18} cm^{-2} are sufficient to promote full oxidation. Further studies are needed to decouple the effects of short-lived and long-lived species on the formation of the Cys-SO₃H.

Cys-SNO formation is dependent on the presence of NO_{aq} . As the gap increases from 1 mm to 10 mm, there is a small increase in the saturated density of NO_{aq} from $4 \times 10^{12} \text{ cm}^{-3}$ to $5 \times 10^{12} \text{ cm}^{-3}$ though the fluence of NO decreases (from $4 \times 10^{17} \text{ cm}^{-2}$ at 1 mm to $2 \times 10^{17} \text{ cm}^{-2}$ at 10 mm). Higher air entrainment in the larger gap leads to conversion of NO to HNO_x in reactions with H and a third body. HNO_x hydrolyzes after solvation to regenerate NO_{aq} (equations (13) and (14)), which contributes to the slight rise in NO_{aq} density as the air gap increases. As the increase in NO_{aq} concentration between the smaller and larger gap is not large, it is more likely that as the gap increases, the reduction in O, OH, and NO fluences, and the resulting aqueous ROS concentrations, contribute to a decrease in competition for reactions at the thiol radical site and a higher rate of formation of Cys-SNO. These trends suggest that increasing the air gap could be a control mechanism if nitrosylated cysteine is the desired product.

Cystine is the only stable product that is not significantly affected by changing the gap. Cystine forms quickly after initial H abstraction from the thiol group (equations (15)–(17)), which indicates that the flux of RONS from the plasma to the liquid is sufficient to initiate cysteine oxidation for all gaps. This result suggests that fluences of RONS on the order of 10^{18} cm^{-2} are greater than needed to promote H abstraction, though the percentage depletion of the initial cysteine molecule may decrease at larger gaps. As such, gap size can be used as a control parameter to select for desired cysteine

oxidation products. However, if complete conversion of native cysteine to oxidized products is desired, gap size may not be the most effective operating parameter.

7.3. Oxygen inlet flowrate

To determine the consequences of ROS fluxes produced by the He/N₂/O₂ COST-jet on the formation of cysteine oxidation products, the inlet mole fraction of oxygen was varied while keeping the inlet mole fraction of nitrogen ($f_{\text{N}_2} = 0.8\%$) and the total inlet flow rate (1010 sccm) constant. The gas-phase densities of a selection of RONS as a function of position in the reactor (and gap) are shown in figure 9 for oxygen inlet flow rates from 1–30 sccm, corresponding to O₂ mole fractions of 0.1%–3%.

As oxygen inlet flow rate increases from 1 sccm ($f_{\text{O}_2} = 0.1\%$) to 8 sccm ($f_{\text{O}_2} = 0.8\%$) there is an increase in gas-phase RONS production. O and NO have maximum densities of $5.6 \times 10^{15} \text{ cm}^{-3}$ and $6 \times 10^{14} \text{ cm}^{-3}$ for $f_{\text{O}_2} = 0.1\%$. For O₂ inlet mole fractions higher than 0.1%, the densities of O and NO begin to decrease as O is consumed by three-body reactions in favor of O₃ production. There is a monotonic increase in O₃ production as O₂ inlet flow rate increases. As the level of water impurity is kept constant, the amount of OH produced in the gas-phase is not greatly affected.

The smallest density of O is produced when the inlet oxygen mole fraction is $f_{\text{O}_2} = 0.1\%$ and the smallest density of NO is produced when $f_{\text{O}_2} = 3\%$. At low flow rates under low power conditions where the fractional dissociation of O₂ is low, there is simply not enough O₂ in the inlet to produce high densities of O. At high inlet O₂ fractions, the consumption of O by three-body processes competes with the consumption of O by reactive nitrogen species to form NO. To maximize both O and NO production in the gas phase, the inlet O₂ fraction must be high enough to produce sufficient O by dissociation, but low enough so that losses of O to O₃ are not dominant.

Although the highest density of O is produced in the gas-phase when the O₂ inlet mole fraction is $f_{\text{O}_2} = 0.8\%$, the highest density of O_{aq} ($2 \times 10^{11} \text{ cm}^{-3}$) occurs when the O₂ inlet fraction is $f_{\text{O}_2} = 0.2\%$. For these conditions, O₂ mole fractions higher than 0.2% result in significant consumption of O in favor of O₃ production in the air gap. The highest densities of OH_{aq} ($6.4 \times 10^{13} \text{ cm}^{-3}$) and $\text{H}_2\text{O}_{2\text{aq}}$ ($1.1 \times 10^{16} \text{ cm}^{-3}$) are also produced at 0.2% inlet O₂. Losses of NO are not as large as loss of O in the air gap and so the highest NO_{aq} density ($5.5 \times 10^{12} \text{ cm}^{-3}$) occurs at $f_{\text{O}_2} = 0.8\%$, when the gas-phase NO production is highest.

Fluences after five minutes of plasma treatment of select RONS that are responsible for the formation of cysteine oxidation products are shown in figure 10(a) for different inlet O₂ fractions. The densities of cysteine and its oxidation products after five-minutes of plasma treatment are shown in figure 10(b). As O₂ inlet fraction increases, depletion of cysteine decreases from over 99% at the lowest O₂ fraction to about 84% at the highest O₂ fraction. Low O₂ inlet fractions yield higher fluences of RONS (O_{aq} , OH_{aq} , $\text{HO}_{2\text{aq}}$) that contribute to hydrogen abstraction from

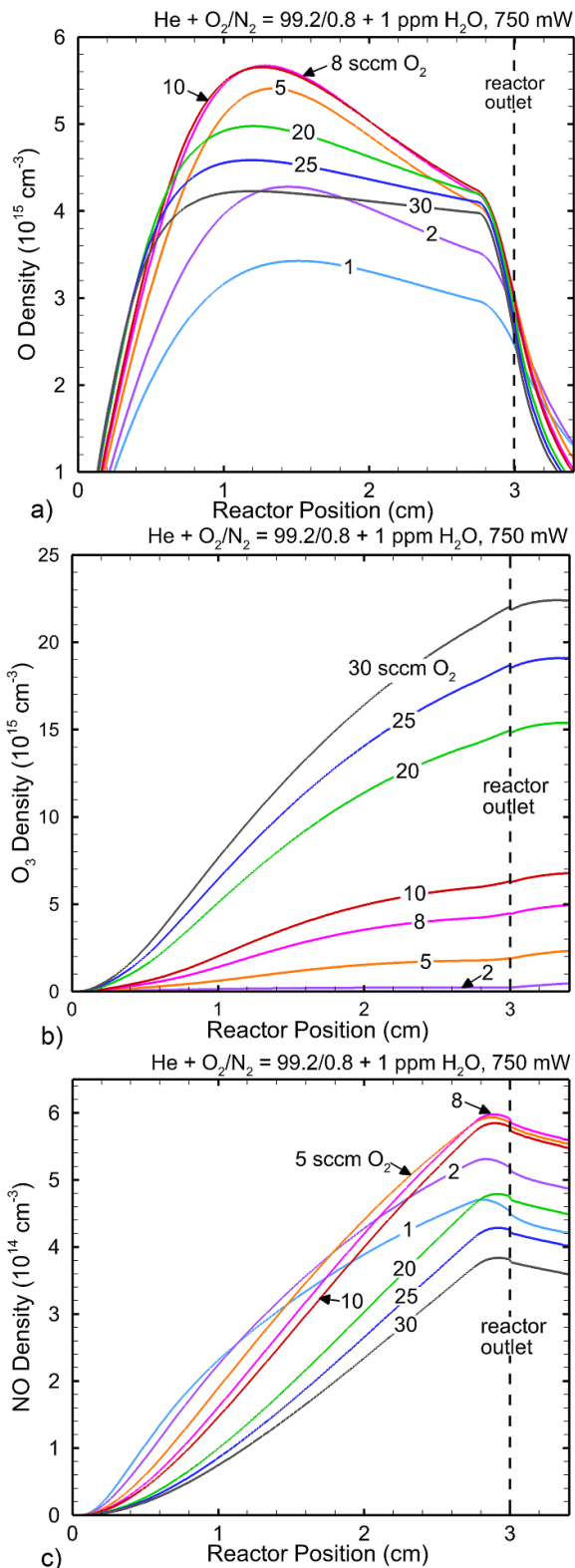


Figure 9. Densities of plasma-produced RONS as a function of O₂ position in the reactor and gap, and O₂ flow rate. (a) O, (b) O₃ and (c) NO.

the thiol site (equations (16)–(18)). As the O₂ inlet fraction increases from 0.1% to 3%, the fluence of atomic O decreases from $4.7 \times 10^{18} \text{ cm}^{-2}$ to $2.9 \times 10^{18} \text{ cm}^{-2}$ as O is consumed in favor of O₃. The maximum O fluence is

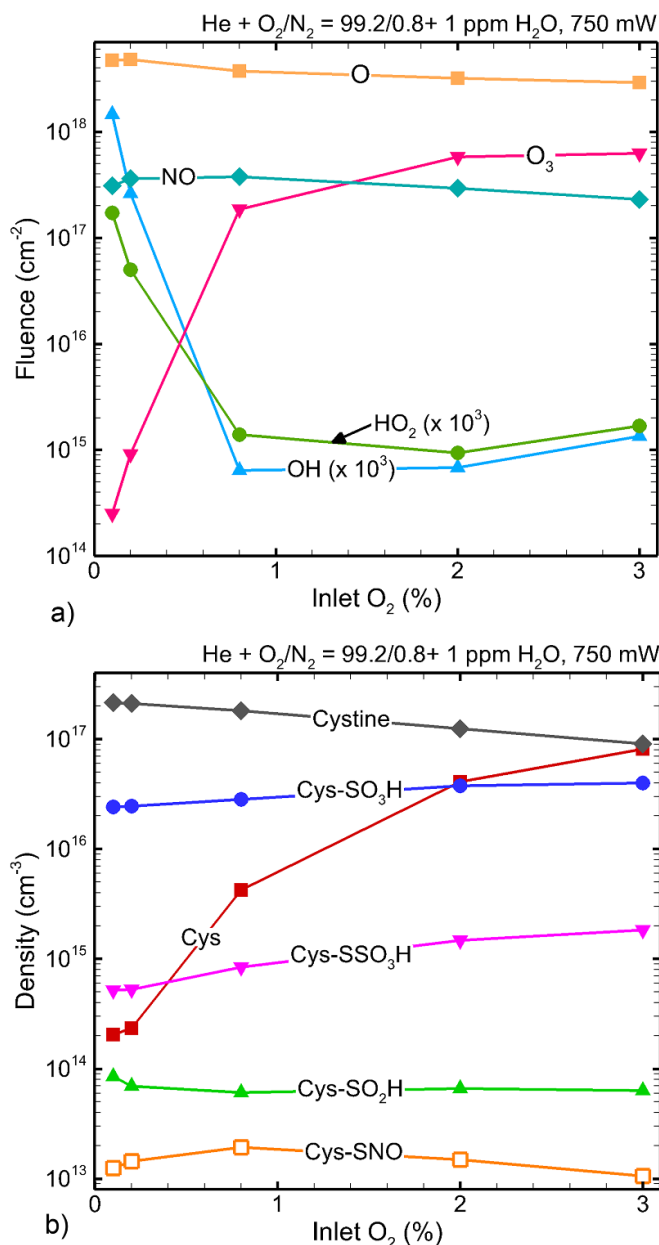


Figure 10. Reactant properties as a function of O₂ inlet fraction after five minutes of treatment by COST-jet sustained in He/N₂O₂. (a) Fluences of select ROS into liquid and (b) cysteine oxidation products.

$4.8 \times 10^{18} \text{ cm}^{-2}$ at $f_{\text{O}_2} = 0.2\%$. OH and HO₂ have maximum fluences of $1.5 \times 10^{15} \text{ cm}^{-2}$ and $1.7 \times 10^{14} \text{ cm}^{-2}$ for $f_{\text{O}_2} = 0.1\%$.

As O₂ inlet fraction increases from 0.1% to 0.8%, the fluence of O₃ increases by three orders of magnitude ($2.5 \times 10^{14} \text{ cm}^{-2}$ – $1.9 \times 10^{17} \text{ cm}^{-2}$) as increased density of O₂ leads to increased O₃ formation through three-body processes. At the same time, fluences of HO₂ and OH also suffer 2–3 orders of magnitude decreases. HO₂ is formed predominantly by third-body assisted reactions of H with O₂ in the gas phase. OH is formed predominantly in the gas-phase by single replacement reactions of HO₂ with O. As O₂ inlet increases and O and O₂ are depleted by O₃ production, HO₂ and OH

production also decrease. Increasing O_2 inlet fraction has little effect on the fluence of NO ($3.1 \times 10^{17} \text{ cm}^{-2}$ at 0.1% O_2 and $2.3 \times 10^{17} \text{ cm}^{-2}$ at 3% O_2), which indicates that the production of NO is limited by the inlet fraction of N_2 under these low power conditions.

With an increase in O_2 inlet fraction, the fluence of O_3 onto the liquid increases. There is a higher rate of formation of Cys-SOH through the intermediate product Cys-SOH₂, which regenerates O_{2aq} and OH_{aq} from O_{3aq} (equation (28)). OH_{aq} converts Cys-SOH to Cys-SO₂H (equation (29)). When the fluence of OH to the liquid decreases (with increasing O_2 inlet fraction), Cys-SOH is not converted to Cys-SO₂H as readily. However, OH fluences of at least $6 \times 10^{11} \text{ cm}^{-2}$ are sufficient to promote formation of the second oxidation state with densities on the order of 10^{14} cm^{-3} .

Though there is a decrease in Cys-SO₂H production from the lowest inlet O_2 fraction to the highest, there is an increase in final Cys-SO₃H density ($2.4 \times 10^{16} \text{ cm}^{-3}$ at $f_{O_2} = 0.2\%$ to $3.9 \times 10^{16} \text{ cm}^{-3}$ at $f_{O_2} = 3\%$). Though the fluence (and aqueous production) of O and OH suffer at high O_2 inlet fractions, Cys-SO₂H can also be converted to Cys-SO₃H by O_{2aq} and H_2O_{2aq} (equations (37) and (38)). Increasing O_2 inlet fraction will monotonically increase O_2 fluence and decrease H_2O_2 fluence. Though the fluences of O, OH, and H_2O_2 are reduced, the increase in O_2 fluence and subsequent increase in generation of O_{2aq} is sufficient to sustain conversion to the final oxidation product. ROS (O_{aq} , OH_{aq}) that originate in the liquid rather than the plasma have some contribution to the formation of Cys-SO₃H [46].

The Cys-SSO₃H formation pathway also requires O_{2aq} (equations (19)–(25)). As the densities of other aqueous RONS (O_{aq} , OH_{aq}) decrease with increasing inlet O_2 , formation of Cys-SSO₃H becomes more viable due to increasing densities of O_{2aq} . Reduction in RONS concentrations also reduces competition between reactions resulting in thiol radical sites (equations (15)–(17)) and reactions of the native cysteine molecule to form cystine (equation (18)). The final density of Cys-SSO₃H is $5.2 \times 10^{14} \text{ cm}^{-3}$ for $f_{O_2} = 0.2\%$ and $1.8 \times 10^{15} \text{ cm}^{-3}$ for $f_{O_2} = 3\%$.

As Cys-SNO formation is dependent upon NO_{aq} (reaction (36) in table 3), production of Cys-SNO is expected to be highest when the NO_{aq} production is highest ($f_{O_2} = 0.8\%$, when the NO fluence is also highest). The final Cys-SNO density is $1.9 \times 10^{13} \text{ cm}^{-3}$ when $f_{O_2} = 0.8\%$ and $1.4 \times 10^{13} \text{ cm}^{-3}$ when $f_{O_2} = 0.2\%$ (base case conditions). Cys-SNO production suffers at higher O_2 inlet fractions, though it is not as greatly affected by increasing O_2 flow rate as other oxidation products. This lack of sensitivity results from the fluence of NO not being as greatly affected by changing O_2 inlet fraction when the N_2 inlet fraction is held constant. As the rate coefficient for the formation of Cys-SNO at a thiol radical site is 2–3 orders of magnitude smaller than the rate coefficient of other oxidation products with the thiol radical site (reaction (36) in table 3), increased Cys-SNO production likely requires NO fluences to be orders of magnitude higher. However, NO fluences on the order of a few times 10^{17} are sufficient to produce Cys-SNO with densities on the order of 10^{13} cm^{-3} .

Cystine production is reduced as inlet O_2 increases ($2.1 \times 10^{17} \text{ cm}^{-3}$ at $f_{O_2} = 0.1\%$ to $9 \times 10^{16} \text{ cm}^{-3}$ at $f_{O_2} = 3\%$). At $f_{O_2} = 0.2\%$, when O_{aq} and OH_{aq} densities are highest (and O fluence is highest), thiol radical production occurs most readily by reaction of cysteine with O_{aq} and OH_{aq} (equations (15) and (16)). When densities of thiol radical sites are high, the fast conversion of two thiol radical sites to cystine occurs more quickly than other ROS can react to form oxidation products (equation (18)). When fluences of ROS are reduced, the production of cystine decreases. Less RONS are available to participate in H abstraction, resulting in a lower density of thiol radical sites. Competition between RONS reactions that form oxidation products and the near immediate reaction of two thiol radical sites to form cystine is reduced due to the lower density of thiol radical sites. More thiol radical sites can be oxidized. The production of Cys-SO₃H is increased due to the increase in O_{2aq} discussed above, though depletion of the native cysteine molecule is reduced at higher O_2 inlet fractions. Total fluences of H-abstracting RONS on the order of 10^{18} cm^{-2} are sufficient to promote H-abstraction that results in at least 84% depletion of the native cysteine molecule.

Control of hydrogen abstraction from cysteine is critical if oxidation products are preferred over the formation of cystine. If full conversion of the cysteine to oxidation products is desired, lower fluences of plasma-produced RONS for longer treatment times may be preferable. If nitrosylated products are also desired, the gas-phase production of NO should be maximized while also controlling the rate of thiol radical site formation.

7.4. Nitrogen inlet fraction

N_2 inlet fraction was varied (f_{N_2} , from 0%–5%) while holding the O_2 inlet fraction ($f_{O_2} = 0.2\%$) and the total inlet flow rate (1010 sccm) constant to investigate the consequences of RNS production on cysteine oxidation product formation. Of special interest here is the formation of the nitrosylated product, Cys-SNO. Maximizing NO additions to organic molecules may be desirable for applications in wound healing and cancer treatment. For example, the presence of NO during wound treatment lowers risk of infection and wound complication by promoting increased cell motility, providing anti-bacterial effects, and influencing gene regulation [59]. Final fluences of select RONS that contribute to the formation of cysteine oxidation products as a function of inlet N_2 fraction are shown in figure 11(a). The final densities of cysteine oxidation products as a function of f_{N_2} are shown in figure 11(b).

Increasing the N_2 flow rate while holding the O_2 flow rate constant increases the density of NO_x species produced in the gas phase and decreases the fluence of ROS (O, OH, HO_2) onto the liquid. O is consumed by NO_x formation while formation of HO_2 and OH require O, O_2 , and H_2O dissociation products such as H. Under low power conditions, O_2 and N_2 will be preferentially dissociated over H_2O . The maximum density of gas-phase NO produced is about $5 \times 10^{14} \text{ cm}^{-3}$ for $f_{N_2} = 1\%$ or higher. Increasing the N_2 fraction beyond 1% does not result in significant increases in the NO density when the O_2

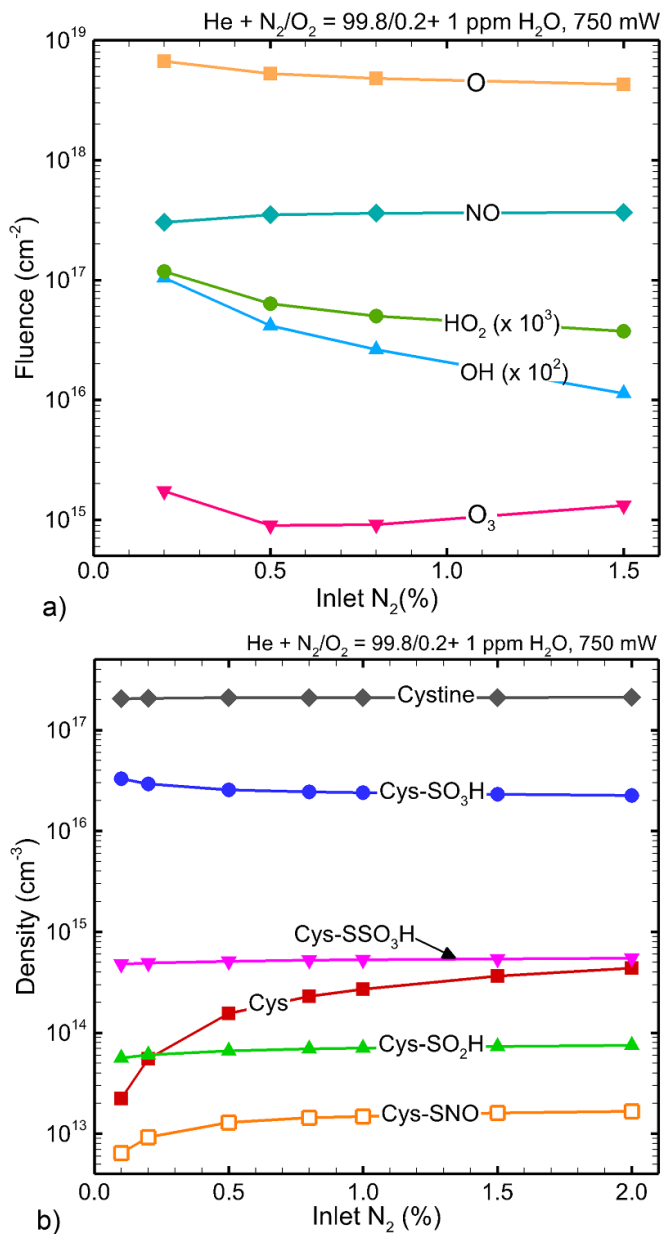


Figure 11. Reactant properties as a function of N_2 inlet fraction after five minutes of treatment by COST-jet sustained in $He/N_2/O_2$. (a) Fluences of select ROS into liquid and (b) cysteine oxidation products.

inlet fraction is held constant at $f_{O_2} = 0.2\%$. The fluence of NO to the liquid is also not terribly sensitive to f_{N_2} (around $3 \times 10^{18} cm^{-2}$ for all f_{N_2}). At this flow rate, production of NO is limited by power and the production of O atoms and not the availability of N_2 . The production of the Cys-SNO product is also not significantly increased for N_2 inlet fractions higher than 1%. The maximum Cys-SNO density after five minutes of plasma treatment is $1.5\text{--}1.6 \times 10^{13} cm^{-3}$.

Varying N_2 inlet fraction while holding O_2 inlet fraction constant results in more depletion of the native cysteine molecule than when O_2 inlet fraction is varied. Varying N_2 inlet fraction results in near complete depletion of the native

cysteine molecule for all N_2 inlet fractions, whereas only 84% of the cysteine molecule was depleted for large values of f_{O_2} . When N_2 inlet fraction is varied with the O_2 inlet fraction being low, the production of O_3 by three-body processes does not deplete O . The fluence of O_3 stays low (around $10^{15} cm^{-2}$) while the fluences of O , OH , and HO_2 remain high enough ($5\text{--}6 \times 10^{18} cm^{-2}$) that hydrogen abstraction from the thiol group (equations (16)–(18)) dominates. The high density of thiol radical sites promotes rapid formation of cystine, resulting in a near constant density of cystine ($1 \times 10^{17} cm^{-3}$) regardless of the N_2 inlet fraction. Since the fluences of ROS remain high as the inlet N_2 increases, and formation of oxidation products Cys- SO_2H , Cys- SO_3H , and Cys- SSO_3H depend only on ROS, not RNS, the final densities of these products are not sensitive to varying N_2 inlet fraction at constant O_2 . The variation in these species is $6\text{--}7 \times 10^{13} cm^{-3}$ Cys- SO_2H , $2\text{--}3 \times 10^{16} cm^{-3}$ Cys- SO_3H , and $5 \times 10^{14} cm^{-2}$ Cys- SSO_3H over the range of f_{N_2} when there is 0.2% O_2 in the inlet.

Increasing f_{N_2} beyond 0.2% does not result in a significant change in Cys-SNO production, as the fluence of NO ($3 \times 10^{18} cm^{-2}$) is limited by the O_2 inlet fraction. As discussed in the previous section, NO fluences on the order of a few times $10^{17} cm^{-2}$ result in Cys-SNO densities on the order of $10^{13} cm^{-3}$. Higher production of Cys-SNO requires higher NO fluence. Higher NO fluence could potentially be achieved by adjusting the N_2 inlet fraction and the O_2 inlet fraction together.

8. Concluding remarks

A reaction mechanism for the CAP treatment of cysteine in water was developed and applied to the investigation of cysteine oxidation and production of nitrosylated products using a global plasma- and liquid-chemistry model. The reaction mechanism was validated against experimental data for COST-jets sustained in He/H_2O and He/O_2 treating cysteine in water. Both gas mixtures result in depletion of the native cysteine molecule while promoting full oxidation to Cys- SO_3H . As the presence of NO and its incorporation into oxidation products is often desirable for wound treatment applications, experiments that treated cysteine solution with a COST-jet sustained in $He/N_2/O_2$ mixtures were performed. Small amounts of nitrosylated Cys-SNO are formed with He/H_2O and He/O_2 due to mixing of the effluent of the COST-jet with the ambient air. Experimental results showed that the nitrosylated Cys-SNO product is produced in much higher quantities after treatment using the $He/N_2/O_2$ mixture due to the controlled and larger production of NO_x .

The validated reaction mechanism and model were used to investigate reaction pathways and mechanisms contributing to the oxidation of cysteine by the COST-jet sustained in $He/N_2/O_2$ mixtures. Results indicate that some selectivity over some oxidation products can be achieved through changing plasma operating parameters such as gap distance and inlet gas flow rate of O_2 and N_2 . The oxidation of the cysteine molecule is sensitive to the gas-phase production of

ROS responsible for the initiating hydrogen abstraction step. If the flux of ROS to the liquid is too high, hydrogen abstraction occurs too quickly and formation of cystine dominates over formation of oxidation products. If the Cys-SNO product is desired, the inlet fraction of N₂ should be increased though tuning other operating parameters (i.e. rf power, total flow rate) may be more effective in selecting for the nitrosylated product.

Only reactions at the cysteine thiol (–SH) site were considered in this work, as the thiol site is the most reactive site on the cysteine molecule. However, hydrogen abstraction can occur at the amino site, along the alkane backbone, or at the carboxyl site as well. Future work should consider whether contributions from these sites also play important roles in the oxidation of the cysteine molecule, as these groups are common in living organisms. Oxidation at sites other than the thiol site on other molecules will contribute to, for example, bacterial inactivation due to oxidative stress.

Cell media solutions usually contain an array of organic and inorganic molecules (i.e. vitamins, proteins) that also likely consume plasma-produced RONS, and with which cysteine derived radical species may react. The fundamental processes discussed in this investigation of RONS reacting with cysteine would be components of that larger, more complex reaction mechanism. We expect that initiating reactions of RONS with other organic molecules will be similar to those discussed here for cysteine. The greatest uncertainty is then reactions of those activated molecules with other organic molecules, leading to structures analogous to cystine or cross-linked-like molecules.

Data availability statement

The data that support the findings of this study are either contained within this paper or available from the corresponding author upon reasonable request.



Acknowledgments

This work was supported by the U.S. National Science Foundation (PHY-2020010, CBET-2032604). This material was also based upon work supported by the U.S. Department of Energy, Office of Science, Office of Fusion Energy Sciences under Award No. DE-SC0020232. The experimental work was performed in part by the Molecular Education, Technology and Research Innovation Center (METRIC) at North Carolina State University, which is supported by the State of North Carolina, USA.

Conflict of interest

The authors have no conflicts of interest to disclose.

ORCID iDs

Jordyn Polito  <https://orcid.org/0000-0003-3409-6007>
 María J Herrera Quesada  <https://orcid.org/0000-0002-8623-550X>
 Katharina Stapelmann  <https://orcid.org/0000-0002-2116-2661>
 Mark J Kushner  <https://orcid.org/0000-0001-7437-8573>

References

- [1] Schlegel J, Körtzer J and Boxhammer V 2013 *Clin. Plasma Med.* **1** 2–7
- [2] Keidar M, Shashurin A, Volotskova O, Ann Stepp M, Srinivasan P, Sandler A and Trink B 2013 *Phys. Plasmas* **20** 057101
- [3] Kramer A et al 2013 *Clin. Plasma Med.* **1** 11
- [4] Kaushik N, Mitra S, Baek E J, Nguyen L N, Bhartiya P, Kim J H, Choi E H and Kaushik N K 2023 *J. Adv. Res.* **43** 59
- [5] Nicol M K J et al 2020 *Sci. Rep.* **10** 1
- [6] Van Gils C A J, Hofmann S, Boekema B K H L, Brandenburg R and Bruggeman P J 2013 *J. Phys. D: Appl. Phys.* **46** 175203
- [7] Weltmann K D, Kinde E, Von Woedtke T, Hähnel M, Stieber M and Brandenburg R 2010 *Pure Appl. Chem.* **82** 1223
- [8] Winter J, Wende K, Masur K, Iseni S, Dünnbier M, Hammer M U, Tresp H, Weltmann K D and Reuter S 2013 *J. Phys. D: Appl. Phys.* **46** 295401
- [9] Fridman G, Peddinghaus M, Ayan H, Fridman A, Balasubramanian M, Gutsol A, Brooks A and Friedman G 2006 *Plasma Chem. Plasma Process.* **26** 425
- [10] Reuter S, Von Woedtke T and Weltmann K D 2018 *J. Phys. D: Appl. Phys.* **51** 233001
- [11] Graves D B 2012 *J. Phys. D: Appl. Phys.* **45** 263001
- [12] Von Woedtke T, Schmidt A, Bekeschus S, Wende K and Weltmann K-D 2019 *In Vivo (Brooklyn)* **33** 1011
- [13] Takai E, Kitamura T, Kuwabara J, Ikawa S, Yoshizawa S, Shiraki K, Kawasaki H, Arakawa R and Kitano K 2014 *J. Phys. D: Appl. Phys.* **47** 285403
- [14] Lackmann J-W, Bruno G, Jablonowski H, Kogelheide F, Offerhaus B, Held J, Schulz-von der Gathen V, Stapelmann K, von Woedtke T and Wende K 2019 *PLoS One* **14** e0216606
- [15] Sies H 1999 *Free Radic. Biol. Med.* **27** 916
- [16] Yang H, Lundbäck P, Ottosson L, Erlandsson-Harris H, Venereau E, Bianchi M E, Al-Abed Y, Andersson U and Tracey K J 2021 *Mol. Med.* **27** 58
- [17] Heusler T, Bruno G, Bekeschus S, Lackmann J-W, von Woedtke T and Wende K 2019 *Clin. Plasma Med.* **14** 100086
- [18] Wende K, Nasri Z, Striesow J, Ravandeh M, Weltmann K-D, Bekeschus S and von Woedtke T 2022 *IEEE Int. Conf. on Plasma Science (ICOPS) 1* (IEEE)
- [19] Poole L B 2015 *Free Radic. Biol. Med.* **80** 148
- [20] Giles G I, Nasim M J, Ali W and Jacob C 2017 *Antioxidants* **6** 38
- [21] Bruno G, Heusler T, Lackmann J W, von Woedtke T, Weltmann K D and Wende K 2019 *Clin. Plasma Med.* **14** 100083
- [22] Ali A A, Coulter J A, Ogle C H, Migaud M M, Hirst D G, Robson T and McCarthy H O 2013 *Biosci. Rep.* **33** e00031

- [23] Belge C, Massion P B, Pelat M and Balligand J L 2005 *Ann. New York Acad. Sci.* **1047** 173
- [24] Paulsen C E and Carroll K S 2013 *Chem. Rev.* **113** 4633
- [25] Wende K, Bruno G, Lalk M, Weltmann K D, Von Woedtke T, Bekeschus S and Lackmann J W 2020 *RSC Adv.* **10** 11598
- [26] Wende K, Von Woedtke T, Weltmann K D and Bekeschus S 2018 *Biol. Chem.* **400** 19
- [27] Kogelheide F, Kartaschew K, Strack M, Baldus S, Metzler-Nolte N, Havenith M, Awakowicz P, Stapelmann K and Lackmann J W 2016 *J. Phys. D: Appl. Phys.* **49** 084004
- [28] Sremački I, Bruno G, Jablonowski H, Leys C, Nikiforov A and Wende K 2021 *Plasma Sources Sci. Technol.* **30** 095018
- [29] Forman H J, Maiorino M and Ursini F 2010 *Biochemistry* **49** 835
- [30] Lackmann J W et al 2018 *Sci. Rep.* **8** 1
- [31] Bekeschus S, Schmidt A, Weltmann K D and von Woedtke T 2016 *Clin. Plasma Med.* **4** 19
- [32] Golda J et al 2016 *J. Phys. D: Appl. Phys.* **49** 084003
- [33] Reuter S, Niemi K, Schulz-Von Der Gathen V and Döbele H F 2009 *Plasma Sources Sci. Technol.* **18** 015006
- [34] Reuter S, Winter J, Schmidt-Bleker A, Schroeder D, Lange H, Knake N, Schulz-Von Der Gathen V and Weltmann K D 2012 *Plasma Sources Sci. Technol.* **21** 034006
- [35] Adams K J et al 2020 *J. Proteome Res.* **19** 1447
- [36] Lietz A M and Kushner M J 2016 *J. Phys. D: Appl. Phys.* **49** 425204
- [37] Kruszelnicki J, Lietz A M and Kushner M J 2019 *J. Phys. D: Appl. Phys.* **52** 355207
- [38] Stancampiano A, Bocanegra P E, Dozias S, Pouvesle J M and Robert E 2021 *Plasma Sources Sci. Technol.* **30** 015002
- [39] Bhoj A N and Kushner M J 2006 *J. Phys. D: Appl. Phys.* **39** 1594
- [40] Dorai R and Kushner M J 2003 *J. Phys. D: Appl. Phys.* **36** 666
- [41] Tian W and Kushner M J 2014 *J. Phys. D: Appl. Phys.* **47** 475203
- [42] Wenske S, Lackmann J W, Busch L M, Bekeschus S, von Woedtke T and Wende K 2021 *J. Appl. Phys.* **129** 193305
- [43] Polito J, Denning M, Stewart R, Frost D and Kushner M J 2022 *J. Vac. Sci. Technol. A* **40** 043001
- [44] NIST Chemical Kinetics Database (available at: <https://kinetics.nist.gov/kinetics/>)
- [45] NDRL/NIST Solution Kinetics Database (available at: <https://kinetics.nist.gov/solutions/>)
- [46] Stapelmann K, Myers B, Quesada M H, Lenker E and Ranieri P J 2021 *J. Phys. D: Appl. Phys.* **54** 434003
- [47] Ellerweg D, Benedikt J, von Keudell A, Knake N and Schulz-von der Gathen V 2010 *New J. Phys.* **12** 013021
- [48] Steuer D, Korolov I, Chur S, Schulze J, Schulz-Von Der Gathen V, Golda J and Böke M 2021 *J. Phys. D: Appl. Phys.* **54** 355204
- [49] Myers B, Barnat E and Stapelmann K 2021 *J. Phys. D: Appl. Phys.* **54** 455202
- [50] Golda J, Kogelheide F, Awakowicz P and Von Der Gathen V S 2019 *Plasma Sources Sci. Technol.* **28** 095023
- [51] Brubaker T R, Ishikawa K, Kondo H, Tsutsumi T, Hashizume H, Tanaka H, Knecht S D, Bilén S G and Hori M 2019 *J. Phys. D: Appl. Phys.* **52** 075203
- [52] Xu H, Chen C, Liu D, Wang W, Xia W, Liu Z, Guo L and Kong M G 2019 *Plasma Sci. Technol.* **21** 115502
- [53] Abe K, Kondo H and Arai S 1987 *Agric. Biol. Chem.* **51** 2763
- [54] Schmidt-Bleker A, Bansemmer R, Reuter S and Weltmann K D 2016 *Plasma Process. Polym.* **13** 1118
- [55] Preissing P, Korolov I, Schulze J, Schulz-Von Der Gathen V and Böke M 2020 *Plasma Sources Sci. Technol.* **29** 125001
- [56] Bailey J L and Cole R D 1959 *J. Biol. Chem.* **234** 1733
- [57] Kohl J B, Mellis A T and Schwarz G 2019 *Br. J. Pharmacol.* **176** 554
- [58] Levine R L, Mosoni L, Berlett B S and Stadtman E R 1996 *Proc. Natl Acad. Sci. USA* **93** 15036
- [59] Suschek C V and Opländer C 2016 *Clin. Plasma Med.* **4** 1–8